

Air Force Institute of Technology

AFIT Scholar

Theses and Dissertations

Student Graduate Works

3-2022

Investigation of Additively Manufactured Molybdenum-tungsten-Rhenium Alloys

Randolph T. Abaya

Follow this and additional works at: <https://scholar.afit.edu/etd>



Part of the [Manufacturing Commons](#), and the [Structures and Materials Commons](#)

Recommended Citation

Abaya, Randolph T., "Investigation of Additively Manufactured Molybdenum-tungsten-Rhenium Alloys" (2022). *Theses and Dissertations*. 5430.

<https://scholar.afit.edu/etd/5430>

This Thesis is brought to you for free and open access by the Student Graduate Works at AFIT Scholar. It has been accepted for inclusion in Theses and Dissertations by an authorized administrator of AFIT Scholar. For more information, please contact AFIT.ENWL.Repository@us.af.mil.



**INVESTIGATION OF ADDITIVELY MANUFACTURED MOLYBDENUM-
TUNGSTEN-RHENIUM ALLOYS**

THESIS

Randolph Osbert T. Abaya, Captain, USAF

AFIT-ENY-MS-22-M-276

**DEPARTMENT OF THE AIR FORCE
AIR UNIVERSITY**

AIR FORCE INSTITUTE OF TECHNOLOGY

Wright-Patterson Air Force Base, Ohio

**DISTRIBUTION STATEMENT A.
APPROVED FOR PUBLIC RELEASE; DISTRIBUTION UNLIMITED.**

The views expressed in this thesis are those of the author and do not reflect the official policy or position of the United States Air Force, Department of Defense, or the United States Government. This material is declared a work of the U.S. Government and is not subject to copyright protection in the United States.

AFIT-ENY-MS-22-M-276

INVESTIGATION OF ADDITIVELY MANUFACTURED MOLYBDENUM-
TUNGSTEN-RHENIUM ALLOYS

THESIS

Presented to the Faculty

Department of Aeronautics and Astronautics

Graduate School of Engineering and Management

Air Force Institute of Technology

Air University

Air Education and Training Command

In Partial Fulfillment of the Requirements for the
Degree of Master of Science in Astronautical Engineering

Randolph Osbert T. Abaya, B.S.M.E

Captain, USAF

March 2022

DISTRIBUTION STATEMENT A.
APPROVED FOR PUBLIC RELEASE; DISTRIBUTION UNLIMITED.

AFIT-ENY-MS-22-M-276

INVESTIGATION OF ADDITIVELY MANUFACTURED MOLYBDENUM-
TUNGSTEN-RHENIUM ALLOYS

Randolph Osbert T. Abaya, B.S.M.E
Captain, USAF

Committee Membership:

Maj Ryan Kemnitz, PhD
Chair

Dr. Carl Hartsfield, PhD
Member

Maj John Brewer, PhD
Member

Abstract

The process of creating metal components through additive manufacturing is changing the way different industries can avoid the shortcomings of traditional metal production. Metals such as tungsten, molybdenum, and rhenium have many advantages for different applications, especially when alloyed together. In this study, an additively manufactured alloy containing 70% molybdenum, 25% tungsten, and 5% rhenium (70Mo-25W-5Re) is tested for its strength, ductility, hardness, and porosity.

The 70Mo-25W-5Re alloy is printed through Laser Powder Bed Fusion (LPBF) under different conditions such as printing speed and printing atmosphere. Additionally, the effects of post printing heat treatment are conducted to understand the advantages to its property changes. The printed alloys are subject to flexural loading and its physical characteristics are tested and observed. The alloy is found to be stronger at slower printing speeds which corresponds to a greater input energy density. Additionally, heat treatments acted to improve strength but had little effect on porosity or hardness.

The benefits of the 70Mo-25W-5Re alloy have a potential for real world applications due to its ease in production. The findings of this research demonstrated how readily alloys of these elements can be studied by leveraging additive manufacturing and post processing heat treatments. This technique will encourage research into different combinations of the constituent elements to find promising compositions in the alloy space.

Table of Contents

	Page
Abstract.....	iv
Table of Contents.....	v
List of Figures.....	vii
List of Tables.....	x
I. Introduction.....	1
1.1 Additive Manufacturing.....	2
1.2 Research Outline.....	3
1.2.1 Problem Statement.....	3
1.2.2 Research Questions.....	4
1.2.3 Scope and Methodology.....	4
1.2.4 Assumptions.....	5
1.2.5 Impacts.....	6
II. Background.....	7
2.1 Tungsten and Molybdenum.....	7
2.1.1 Crystallographic Properties.....	7
2.1.2 Alloying.....	8
2.1.3 70% Molybdenum 25% Tungsten 5% Rhenium Alloy (70Mo-25W-5Re).....	10
2.2 Traditional Processing.....	14
2.2.1 Powder Production.....	14
2.2.2 Powder Metallurgy.....	15
2.2.3 Problems with Traditional Metallurgy.....	16
2.3 Additive Manufacturing of Metals.....	16
2.3.1 Advantages of Additive Manufacturing.....	17
2.3.2 Additive Manufacturing Limitations.....	18
2.3.3 Resolving Additive Manufacturing Limitations.....	21
2.4 Summary.....	22
III. Methodology.....	23
3.1 Printing Process.....	23
3.2 Bend Test Preparation.....	25

3.3 Bend Test Procedure	28
3.4 Data processing	30
3.5 Carbon Puck	30
3.6 Data Analysis	32
3.6.1 Fracture Surface Observations.....	32
3.6.2 Hardness Testing	33
3.6.3 Porosity Data	34
3.6.4 Homogeneity Analysis	35
IV. Analysis and Results.....	36
4.1 Bend Test Results.....	36
4.2 Scanning Electron Microscope (SEM) results	49
4.3 Vickers Hardness Test.....	54
4.4 Porosity Analysis.....	55
4.5 Energy Dispersive X-ray Spectroscopy (EDS) results.....	58
4.6 Summary	64
V. Conclusions and Recommendations	66
5.1 Shortcomings.....	66
5.2 Conclusions	66
5.3 Future Recommendations.....	68
Appendix A. Matlab Code	69
A.1 Stress Strain Data Processing for 1600 °C Heat Treated and Non-Heat-Treated Samples	69
A.2 Stress Strain Processing for 2000 °C and 2200 °C Heat Treated Samples	88
A.3 Heat Treatment Temperature vs Stress and Strain Code.....	95
Bibliography	105

List of Figures

Figure 2.1 Bravais Crystal Lattice [14].....	8
Figure 2.2 Tensile properties over a range of temperatures for tungsten (W) and alloy with rhenium (Re) [16]	9
Figure 2.3 Tungsten, molybdenum, rhenium density chart	11
Figure 2.4 Tungsten, molybdenum, rhenium isothermal ternary diagram at 1600 °C	12
Figure 2.5 Molybdenum and tungsten binary phase diagram.....	13
Figure 2.6 Metallographic cross section of porosity from keyhole mode melting [24]	19
Figure 2.7 (a) Porosity effected by printing speed (I) 250 (II) 500 (III) 750 and (IV) 1000 mm/s [26], (b) Porosity effected by laser power (I) 90 (II) 120 and (III)180 W [27]	19
Figure 2.8 (a) SEM image of solid powders on build surface [28], (b) balling effect [29]	20
Figure 3.1 GE Additive/Concept Laser MLab 200R Cusing(R) [33].....	23
Figure 3.2 Printed 70% Mo 25% W 5% Re vertical sample (left) and 45° sample (right).....	25
Figure 3.3 Buehler Ecomet 300 Grinder and Polisher [34]	26
Figure 3.4 Ground 70% Mo 25% W 5% Re vertical sample (left) and 45° sample (right).....	27
Figure 3.5 OmegaLux LMF 3550 Benchtop Muffler Furnace [35].....	28
Figure 3.6 MTS Acumen Electromechanical Test System [36]	29
Figure 3.7 MetLab Metpress A [37]	31
Figure 3.8 Carbon Puck	32
Figure 3.9 Tescan Maia3 Scanning Electron Microscope [38].....	33
Figure 3.10 QATM Qness Hardness Tester [40]	34
Figure 4.1 Average % Strain vs Breaking Stress per Print Speed of 70% Mo 30% W under Argon-Hydrogen and Argon Gas.....	37
Figure 4.2 % Strain vs Breaking Stress of 70% Mo 25% W 5% Re	39

Figure 4.3 Average % Strain vs Breaking Stress per Print Speed of 70% Mo 25% W 5% Re	39
Figure 4.4 Average % Strain vs Breaking Stress per Print Speed of Heat Treated 70% Mo 25% W 5% Re.....	41
Figure 4.5 Stress vs Heat Treatment Time per vertical print speed.....	43
Figure 4.6 Strain vs Heat Treatment Time per vertical print speed.....	43
Figure 4.7 Stress vs Heat Treatment Time per 45° print speed	44
Figure 4.8 Strain vs Heat Treatment Time per 45° print speed	44
Figure 4.9 % Strain vs Breaking Stress of Heat Treated 70% Mo 25% W 5% Re at 2000 °C and 2200 °C	46
Figure 4.10 Average % Strain vs Breaking Stress per Print Speed of Heat Treated 70% Mo 25% W 5% Re at 2000 °C and 2200 °C.....	47
Figure 4.11 Strain vs stress for vertical samples heat treated at 1600 °C and 2000 °C.....	48
Figure 4.12 Strain vs stress for 45° samples heat treated at 1600 °C and 2000 °C	48
Figure 4.13 Strain vs stress for vertical samples heat treated at 1600 °C and 2200 °C.....	49
Figure 4.14 Molybdenum Oxide formed at the fracture surface	50
Figure 4.15 70Mo-25W-5Re fracture surface of the 100 mm/s sample (left) and the 600 mm/s sample (right) at 5.0kx magnitude highlighting different crack sizes	51
Figure 4.16 70Mo-25W-5Re fracture surface of the 100 mm/s sample (left) and the 600 mm/s sample (right) at 1.0kx magnitude highlighting unmelted particles	52
Figure 4.17 70Mo-25W-5Re fracture surface of the 300 mm/s sample heat treated at (a) 4 hours (b) 8 hours (c) 12 hours (d) 24 hours highlighting unmelted particles	53
Figure 4.18 Porosity of 70Mo-25W-5Re under a 4-hour treatment with printing speeds of (a) 100 mm/s, (b) 200 mm/s, (c) 300 mm/s, (d) 400 mm/s	56
Figure 4.19 Pore count of a non-heat-treated sample printed at 100 mm per seconds.....	57
Figure 4.20 Characteristic X-ray spectrum of 70Mo-25W-5Re printed at 100 mm/s and heat treated for 4 hours.....	60

Figure 4.21 Phase diagram of 70Mo-25W-5Re printed at (a) 100 mm/s (b) 200 mm/s (c) 300 mm/s (d) 400 mm/s and heat treated for 4 hours 62

Figure 4.22 W phase diagram at (a) No Heat Treatment (b) 1600 °C (c) 2000 °C (d) 2200 °C printed at 400 mm/s 64

List of Tables

Table 1.1 Properties of Tungsten, Molybdenum, and Rhenium [7]	3
Table 4.0.1 Stress vs strain of different printing speeds for 70% Mo 30% W	38
Table 4.2 Average Breaking Stress (MPa) vs % Strain of 70% Mo 25% W 5% Re.....	40
Table 4.3 Average Breaking Stress (MPa) vs % Strain of Heat Treated 70% Mo 25% W 5% Re	42
Table 4.4 Average Breaking Stress (MPa) vs % Strain of Heat Treated 70% Mo 25% W 5% Re	47
Table 4.5 Average Hardness Value of various heat treated 100 mm/s samples.....	54
Table 4.6 Pore count and pores area size of each 70Mo-25W-5Re sample	58
Table 4.7 Average Concentration of Mo, W, and Re at different printing speeds and heat treatment time	59
Table 4.8 Concentration of Mo, W, and Re at different printing speeds, heat treatment time, and heat treatment temperatures	60

INVESTIGATION OF ADDITIVELY MANUFACTURED MOLYBDENUM- TUNGSTEN-RHENIUM ALLOYS

I. Introduction

Tungsten (W), also known as wolfram in other countries, is one of the most heat resistant and densest metals found in nature. This metal was originally recognized as the mineral wolframite from Peter Woulfe, a chemist from England in the 18th century. A couple years later, the tungsten we know today was discovered by Jose and Fausto d'Elhuyar of Spain when they refined the mineral through the process of separating the tungsten from the metal oxide, wolframite. Due to its strength and resistance to high temperature, tungsten is widely used in alloys that require these properties such as drill bits, welding, and even spacecraft operations [1]. Tungsten alone, however, has its faults. It is brittle, which means that to improve its application for dynamic uses, it must be mixed with other metals [2]. This is where metals such as molybdenum and rhenium provide utility.

Like tungsten, molybdenum (Mo) is known for its high melting point. This metal, whose name first derived from the Greek word “molybdos” for lead, was first discovered by the Swedish chemist Carl Wilhelm Scheele and refined to its pure form first by Peter Jacob Hjelm a few years later. Molybdenum is commonly used for alloying to increase an alloy's hardness, strength, and resistance to heat and corrosion. These properties make molybdenum valuable for applications such as engine parts, drills, and heating elements. Interestingly, molybdenum also has a role for biological applications [3]. Given that molybdenum is lighter than tungsten, it becomes advantageous to alloy the two together

to reduce the density of the alloy while leveraging the beneficial effect of solid solution strengthening.

Rhenium (Re) is an important metal for alloying due to its ability to improve ductility and tensile strength. Rhenium, named after the famous Rhine River, was originally speculated to exist since the creation of the periodic table by Dimitri Mendeleev. Its discovery dates to the early 20th century by German scientists Walter Noddack, Otto Berg, and Ida Noddack. Like tungsten and molybdenum, rhenium has a high melting point. With a characteristic like this, rhenium would serve its purpose in equipment such as filaments, grid heaters, and nuclear reactors [4]. With the special qualities molybdenum and rhenium provides, it becomes beneficial for these metals to be alloyed with tungsten.

1.1 Additive Manufacturing

The commercial use of additive manufacturing did not make an appearance until 1987 when the company 3D Systems came up with the process of using ultraviolet light to shape and process a liquid polymer that reacts to that light. This process, known as stereolithography (SL), continued to develop and became widely used for different applications such as prototyping. Additive manufacturing for metals did not become available until the arrival of selective laser sintering (SLS). This process, which came from the DTM corporation, involves using a high-powered laser to heat the metallic grains. The metallic grains would then melt and fuse together to form a solid product. With SLS, the speed and direction at which the laser moves can create unique shapes out

of different metals [5] [6]. These early examples of additive manufacturing helped pave the way with manufacturing unique parts made of different materials.

1.2 Research Outline

1.2.1 Problem Statement

The relatively low cost and ease of additive manufacturing has potential to improve its production across all kinds of applications. The issue that stands, however, is what other metals should be considered when producing a tungsten alloy. Two metals that are considered in the present research are both molybdenum and rhenium. Molybdenum has properties associated with a high melting point and a low thermal expansion coefficient. Rhenium is also associated with having a high melting point as well as high hardness as seen in Table 1.1.

Table 1.1 Properties of Tungsten, Molybdenum, and Rhenium [7]

Property	W	Mo	Re
Atomic Number	74	42	75
Atomic Mass, (g/mol)	183.8	95.9	186.2
Crystal Structure	bcc	bcc	hcp
Density (g/cm ³)	19.25-19.35	10.1-10.3	21.00-21.02
Melting Temperature (°C)	3410-3420	2607-2622	3157-3181
Tensile Strength (MPa)	1670-3900	380-2100	1000-2500
Yield Strength (MPa)	1350-3500	170-2000	280-2350
Young's Modulus of Elasticity (GPa)	340-405	315-343	461-471
Hardness (MPa)	4500-8500	1500-6500	2600-7500

Current alloys have mostly focused on the combination of tungsten and molybdenum and tungsten and rhenium. Meanwhile, the tungsten, molybdenum, rhenium alloy has been rarely studied in this form due to the cost of rhenium. Even fewer is the analysis of additively manufactured alloys of tungsten, molybdenum, and rhenium. Due

to the ease of additive manufacturing compared to traditional alloying, it is worth looking into the creation of such an alloy and analyzing its properties. Understanding its properties could lead to an advantage of quickly and efficiently producing high temperature air and space vehicle structures.

1.2.2 Research Questions

Designing air and space vehicles efficiently will require an understanding of the process and materials used in creating components. If one were to use an additively manufactured alloy of molybdenum and tungsten with a small fraction of rhenium, there needs to be some knowledge on what methods can best replicate a material that can meet mission needs. This leads to the following questions:

- Can a mixture of elemental powders produce a homogeneous mixture through additive manufacturing? Does this affect the alloy's properties?
- How does the molybdenum, tungsten, rhenium alloy compare to the more widely used molybdenum-tungsten alloy? What additional procedures outside of additive manufacturing settings can be done to further improve the alloy's properties?
- What are the effects of heat treatment when applied to a printed alloy? Will factors such as length of heat treatment and temperature play a significant role?

1.2.3 Scope and Methodology

All printed alloys are created on the same additive manufacturing machine. Part of the experimental design includes varying printing speed and the composition of the shield gas atmosphere in which the samples are printed. However, all other conditions remain consistent. A total of three samples are printed per unique printing parameter

combination. This is done to get an average of the samples properties in case there are any outliers. To analyze the stress and strain of each sample, all samples go through a three-point bend test where the applied load is recorded. This data with the dimensions of the sample is used to calculate the strength and strain at fracture of the alloy. After all samples are analyzed for its strength and ductility, its microstructure is studied and its hardness, porosity, and homogeneity are measured on the same equipment and software.

All samples are printed through laser powder bed fusion, specifically with the GE Additive/Concept Laser MLab 200R Cusing. The bend test for these samples is conducted on the MTS Acumen Electromechanical Test System. Additional data gathering equipment used is the scanning electron microscope for microstructure observations and the QATM Qness machine for hardness testing. The software used includes the EDAX team software for homogeneity analysis and the Zeiss software for porosity analysis.

1.2.4 Assumptions

Oxidation from storage may influence the quality of the printed sample. The longer a powder is stored, the more of an influence oxidation can have, thus weakening the final product of the sample [8]. In this study, the printed samples come from differently stored batches of metal powders. However, the production of these samples took place in a fairly short period of time. Therefore, it is assumed that differences due to storage will not be a factor in this research.

Other assumptions include the powder bed thickness being the same and printing parameter specifications being consistent. All samples printed are also set to have a 50 micron hatch spacing with 20 micron layer thickness.

1.2.5 Impacts

Selecting the ideal powder composition, printing speed, and post printing heat treatment process to produce a strong, heat resistant alloy can come a long way with varying Air Force and Space Force missions. The combination of tungsten, molybdenum, and rhenium has potential in supporting nuclear thermal propulsion. During the GE-710 program, a combination of this alloy is seen to have advantages such as high strength, melting point, and ductility in addition to low oxygen permeability. However, higher bond stresses caused by the fuel matrix and alloy during thermal cycling poses as an issue [9]. Comparing the results of these alloys to other additively manufactured alloys can open other research opportunities related to air and space vehicle designs. The results of the heat-treated tungsten, molybdenum, rhenium alloy from this research can also inspire an additional variety of methods such as changing the ratio of each metal powder or heat treatment process.

II. Background

2.1 Tungsten and Molybdenum

Tungsten and molybdenum are highly sought-after materials for different industries. Physical and chemical properties of tungsten and molybdenum such as their high melting points, high tensile strengths, high electrical and thermal conductivities, and high wear resistance makes these materials able to serve many purposes [10] [11]. The biggest difference is that the density of tungsten is much higher than that of molybdenum. All these different properties make tungsten versatile in many applications such as its use in lighting, high temperature equipment, welding, aviation, space aviation, and even in sports and leisure [12]. Like tungsten, molybdenum is commonly used in aviation and aerospace. Its resistance to high temperatures also makes molybdenum a common metal for the nuclear power industry [11]. Understanding the metallurgy and production can provide an insight to how it benefits different purposes and what promises it can hold when it is improved upon.

2.1.1 Crystallographic Properties

There are three crystallographic modifications of tungsten: α -tungsten, β -tungsten, and γ -tungsten. The α -tungsten form has a body centered cubic crystal structure and is the most stable of the three. The β -tungsten form is metastable which means at a certain temperature above 600 °C, the β -tungsten form can convert to the α -tungsten form. As for γ -tungsten, it is a crystal structure of face centered cubic. They are only found in the

sputtered layers and, like β -tungsten, will convert to the α -tungsten form when heated above a certain temperature [12].

At its solid state, molybdenum is crystallized in the body-centered cubic structure where it is at its most stable form. At higher temperatures and pressures, molybdenum is calculated to be in the face-centered cubic structure. Although it is possible for molybdenum to obtain a hexagonal close-packed structure, it would not be stable [13]. The different geometries of these crystal structures can be seen in Figure 2.1. Since both tungsten and molybdenum have similar crystal structures, there should be no complications in combining both metals through alloying.

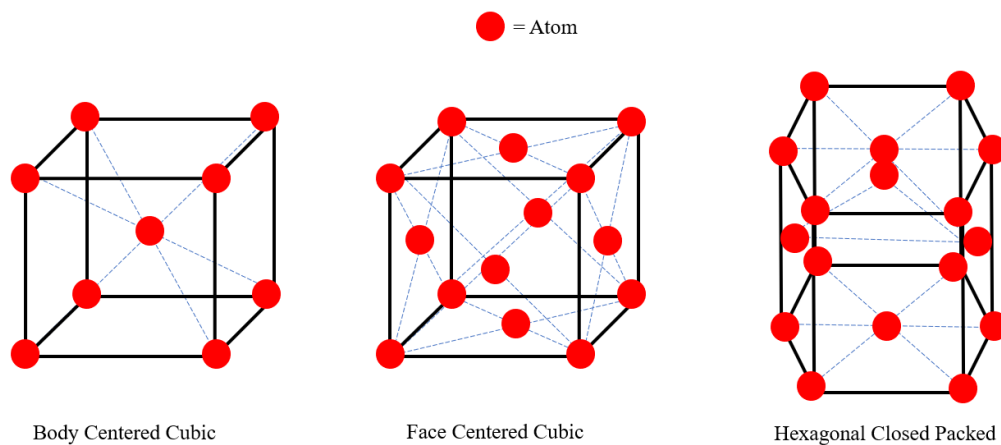


Figure 2.1 Bravais Crystal Lattice [14]

2.1.2 Alloying

Despite the advantages in strength and extreme heat resistance, tungsten alone is not sufficient to accomplish some missions. In colder temperatures, tungsten remains brittle and poses a problem when its strength is required in an arctic environment.

Tungsten is also one of the densest metals on earth, making it difficult for air and space

operations. Alloying other metals with tungsten is a practical solution to circumventing the inherent disadvantages of tungsten.

Tungsten generally reacts well with groups 4 to 7 in the periodic table. This group includes both rhenium and molybdenum [15]. The addition of rhenium into the tungsten and molybdenum alloy is a topic worth studying. Rhenium can improve both tensile strength and ductility. Additionally, rhenium has interesting properties at high temperatures such as increased strength and fatigue fracture prevention [4]. Studies even show that tungsten-rhenium alloys are stronger and harder than pure tungsten over ranging temperatures as seen in Figure 2.2.

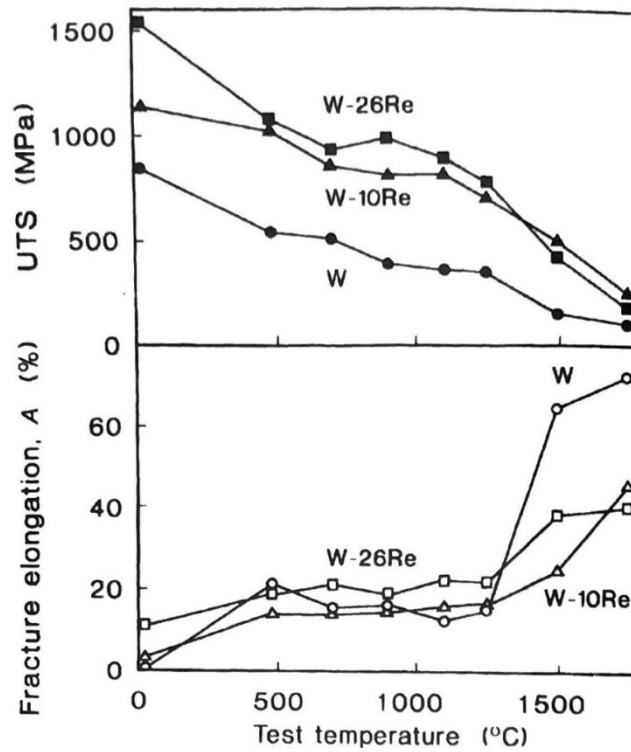


Figure 2.2 Tensile properties over a range of temperatures for tungsten (W) and alloy with rhenium (Re) [16]

Molybdenum is a metal known for its ductility. Mechanically, molybdenum can resist high stress and high strain as well as high temperatures due to having the fifth highest melting point compared to other metals. Despite being generally softer and weaker than tungsten and rhenium, molybdenum is less dense than these two metals. This makes it a more suitable metal that could be applied to air and space applications [17].

2.1.3 70% Molybdenum 25% Tungsten 5% Rhenium Alloy (70Mo-25W-5Re)

In this research, the properties of an alloy containing 70 % molybdenum, 25% tungsten, and 5% rhenium is evaluated. Given the advantage of being a lighter metal compared to tungsten and rhenium, molybdenum is the metal that dominates in presence within the alloy. Figure 2.3 shows the density chart of different combinations of tungsten, molybdenum, and rhenium where density is calculated with equation 2.1 where W is the material and ρ is the density.

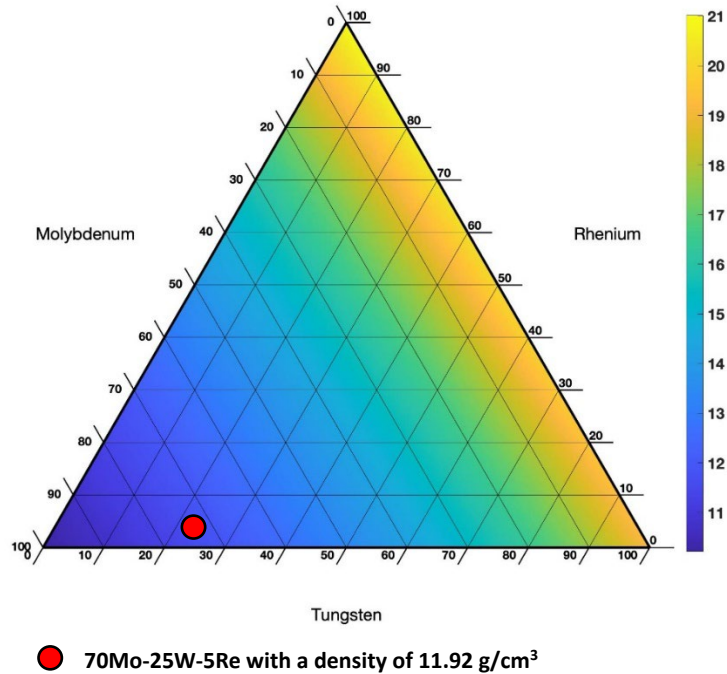


Figure 2.3 Tungsten, molybdenum, rhenium density chart

$$\frac{W_1}{\rho_1} + \frac{W_2}{\rho_2} + \frac{W_3}{\rho_3} = \frac{100}{\rho} \quad (2.1)$$

An alloy that mostly contains rhenium is subject to be very dense as seen from the chart. Rhenium may be dense, but its addition to the alloy has been proven to provide benefits to the alloy's characteristics such as improved ductility and toughness. Instead of omitting the metal entirely, a small percentage is added to the alloy for research.

In addition to density, the ratio of tungsten, molybdenum, and rhenium is chosen to avoid detrimental intermetallic phases during its alloying process. If the alloy were to experience these phases, it risks being a less tough and more corrosive metal. Detrimental

intermetallic phases are more likely to occur at higher concentrations of rhenium as seen in Figure 2.4.

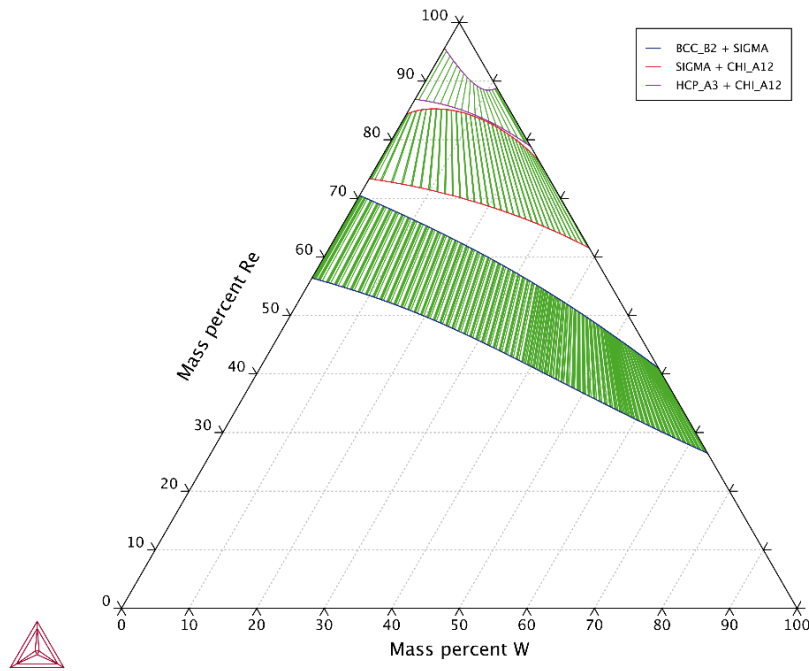


Figure 2.4 Tungsten, molybdenum, rhenium isothermal ternary diagram at 1600 °C

From the isothermal ternary diagram, most of the detrimental intermetallic phases occur when there is a higher concentration of rhenium in the alloy. Molybdenum is able to tolerate the presence of greater concentrations of rhenium without formation of intermetallic phases than tungsten. This motivates the alloy compositions to be comprised primarily of molybdenum rather than tungsten.

Even though molybdenum dominates in concentration of the alloy, there is little concern with how it will blend with tungsten. Figure 2.5 exhibits the binary alloy of tungsten and molybdenum across an array of temperatures. What this figure shows is the

phases that are present depending on the alloy composition and temperature. In this figure, a 0% mass percent of molybdenum indicates a 100% mass percent of tungsten. Below the shaded region is the solid state of the two elements and above that region is the liquid phase. From this graph, the molybdenum and tungsten alloy are an isomorphous system in the shaded region. This means that since both metals are mixable with each other in the liquid state and solid state, there is no expectation of undesirable phases forming.

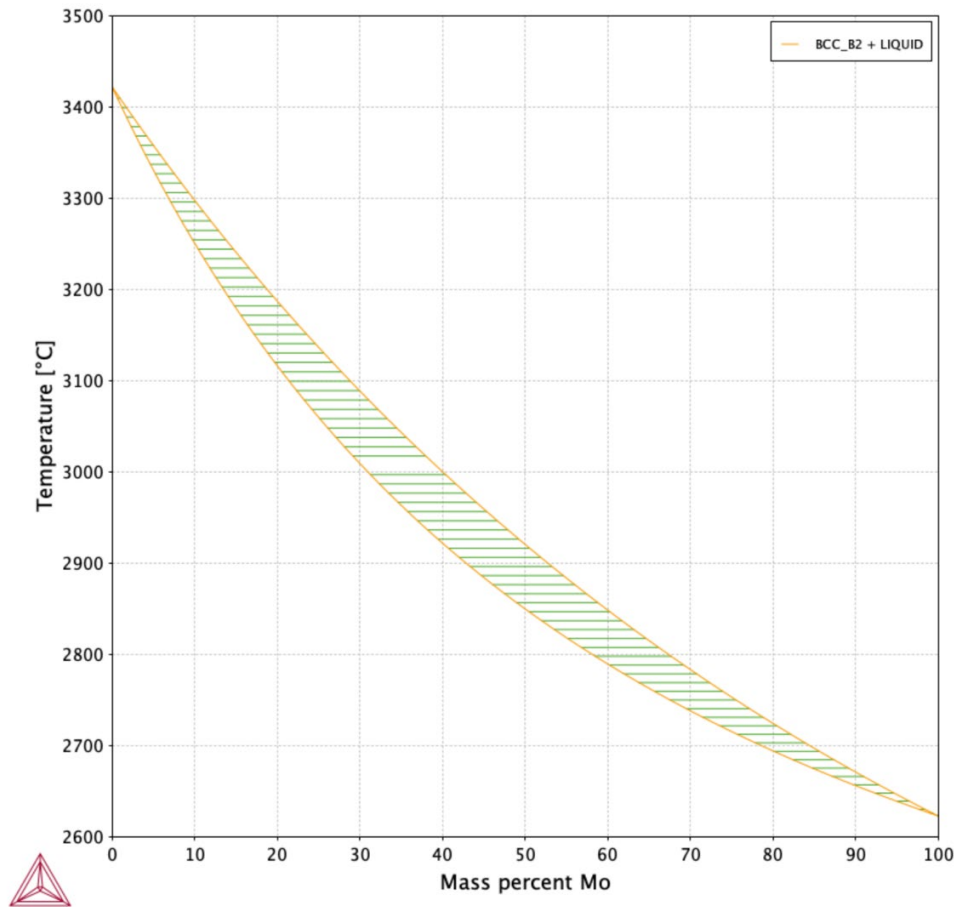


Figure 2.5 Molybdenum and tungsten binary phase diagram

Given what is known about W-Re alloys and W-Mo alloys and their benefits, it is worth understanding the benefits of what a combination of the three metals can provide. Of course, there are numerous combinations of concentrations that can be done. As a start, a study on a 70Mo-25W-5Re alloy can set an idea of what characteristics and promises the material can provide.

2.2 Traditional Processing

Tungsten and molybdenum ores have been mined and processed for centuries, but only began being used for engineering purposes by the mid-19th century [18]. The process of obtaining a functional form of tungsten starts like most metals with mining ores of its naturally stable oxide, WO_3 , in mines. For molybdenum, the metal is most commonly found as its stable sulfide, MoS_2 . These materials then go through the process of transforming from compound raw material into pure metals for manufacturing use.

2.2.1 Powder Production

The production of tungsten powder is crucial for the formation of tungsten materials. The shape and size of the powder can have an influence on the ease of the compacting and sintering process. Therefore, it is important to carefully process the powder to save time with the development of solid tungsten. To produce tungsten powder, the element itself must first be isolated. Tungsten trioxide (WO_3) is the starting compound when it comes to powder production. Hydrogen is used to isolate the tungsten element by a reduction reaction with the oxide. This gas is important since it is used to react with the oxide in the compound.

Using either push-type furnaces or rotary furnaces, the WO_3 material is heated at high temperatures with the hydrogen to produce tungsten powder. These powders typically range from $0.1 \mu\text{m}$ to $100 \mu\text{m}$ in grain diameters. These different grain sizes are affected by the temperature applied, the method of heating, and the quality of the hydrogen used [12].

Like tungsten, having a careful production of molybdenum powders is also important. The powder production of molybdenum runs a similar process with isolating and heating the raw material to create molybdenum powders. Molybdenum being mined starts off as MoS_2 , and it must be converted to technical molybdic oxide (MoO_3) by extracting the sulfur. This process is possible through heating the raw material in furnaces with multiple stages. The reaction with outside oxygen and heat results in technical molybdic oxide. This compound is further refined into pure molybdic oxide through sublimation. In the final process, like tungsten, molybdenum is extracted to its purest form by introducing hydrogen and heat through a rotary furnace. What is left is pure molybdenum powder [19].

2.2.2 Powder Metallurgy

In the traditional method of producing tungsten, powder metallurgy is commonly used. The two main steps are compaction and sintering. The first step of compaction is the process of taking the tungsten powder and compacting it either through the die pressing method or through isostatic pressing. Die pressing involves using a hydraulic or mechanical press while isostatic pressing involves putting the tungsten powder in a mold and subjecting it through hydrostatic pressure. Compacting the tungsten powder is

difficult overall due to the rigidity of the powder. Nevertheless, it is a step required to set up sintering. The sintering process, or heat treatment, of the compacted powder is the step that densifies the tungsten powder into a solid metal. In this process, the temperature and pressure determine how dense the final product will become. The sintering process can either be a direct sintering process or an indirect sintering process. The differences between the processes are the sintering time and temperature. The size of the final product also drives which method of sintering is possible [12].

Molybdenum powders can also go through a similar process of compacting and sintering. The compacting technique and how well the powder is sintered can determine how much of the mechanical properties of molybdenum are retained [20].

2.2.3 Problems with Traditional Metallurgy

The production of tungsten has been refined over the years since its discovery. Despite the current method of compacting and sintering being common, problems still exist in this method. If one desires to have tungsten produced at a specific shape, the fabrication of that shape would require a complex process of adjusting temperatures and formation. The upper and lower temperature limit of the shaping process must be followed, otherwise cracks and splits can develop [12].

2.3 Additive Manufacturing of Metals

Additive manufacturing is a method of creating parts by layers. The formation of these layers and the shape they make is dependent on a 3D model created on a computer. Early development of additive manufacturing involved the creation of parts made of plastic due to its characteristics that make it easy to fabricate. It has since then evolved to

create metal parts through the processes of selective laser sintering (SLS), electron beam melting (EBM), and laser engineering net shaping (LENS). Generally, these processes use a similar approach of using a high-powered laser or electron beam to fully melt a bed of powdered metal. This process binds the powder together and forms a solid metal object. With the ability of the powder bed to move, specific shapes can be created [21].

2.3.1 Advantages of Additive Manufacturing

Additive manufacturing has numerous advantages in the industrial world already. Advantages such as its efficiency, mass customization, on-demand manufacturing, and the ability to modify a design without significant time or cost penalties help push manufacturers to pursue additive manufacturing. In the aerospace industry, parts are already being produced through additive manufacturing across different models of commercial and military aircraft [22].

Tungsten and molybdenum are refractory metals due to their high melting point. The flaw with refractory metals, however, is that they are often subject to aggressive oxidation at high temperatures. Through additive manufacturing, the atmosphere can be controlled in the chamber the alloy is built in to reduce oxidation. Additive manufacturing can also save costs when working with these refractory metals. Through traditional methods, the production of parts with complicated designs becomes expensive through the process of subtracting and joining metals. Further, machining on these hard metals also incurs more cost due to cutting tool wear. Working with these refractory powders is a difficult and laborious process, especially when it comes to sintering and shaping. With additive manufacturing, the shaping is directly done in the machine. The

part being produced rarely needs to be bent or punched to create a specific shape. With the incentives of fewer restrictions to a part design and a shorter lead time, additive manufacturing gains attention from different industries [22] [23].

2.3.2 Additive Manufacturing Limitations

Despite the ease of working with additive manufacturing, the final product is still bound to different flaws. Flaws include porosity, surface roughness, and cracking during and after the printing process.

2.3.2.1 Porosity

Porosity is a common byproduct of metals produced through additive manufacturing. One cause of porosity is a lack of careful control in keyhole mode melting. During keyhole melting, the energy density of the laser beam aimed at the powder bed causes the metal to evaporate. This process leaves a cavity that increases the laser's absorption and allows the laser to reach deeper into the powder bed. If the cavity is unstable, it collapses leaving behind pores such as the ones seen in Figure 2.6 [24]. Porosity can also form from trapped gas. During the atomization process, non-metals such as inert gases do not dissolve with metals in a liquid state. By the time the metal solidifies, the gas entrapped in the metal leaves a void inside the printed part. The machine settings influences porosity sizes as well. Laser power and speed determines how well the fusion between powders can occur [25]. Figure 2.7 demonstrates different pores created from various printing speed and laser power.

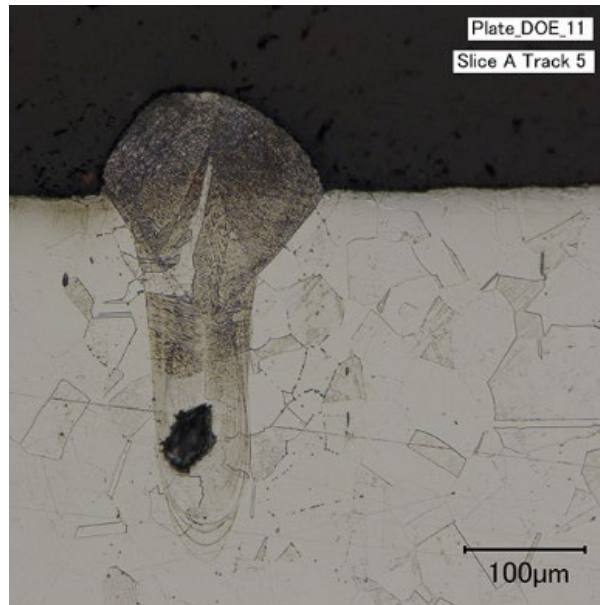


Figure 2.6 Metallographic cross section of porosity from keyhole mode melting [24]

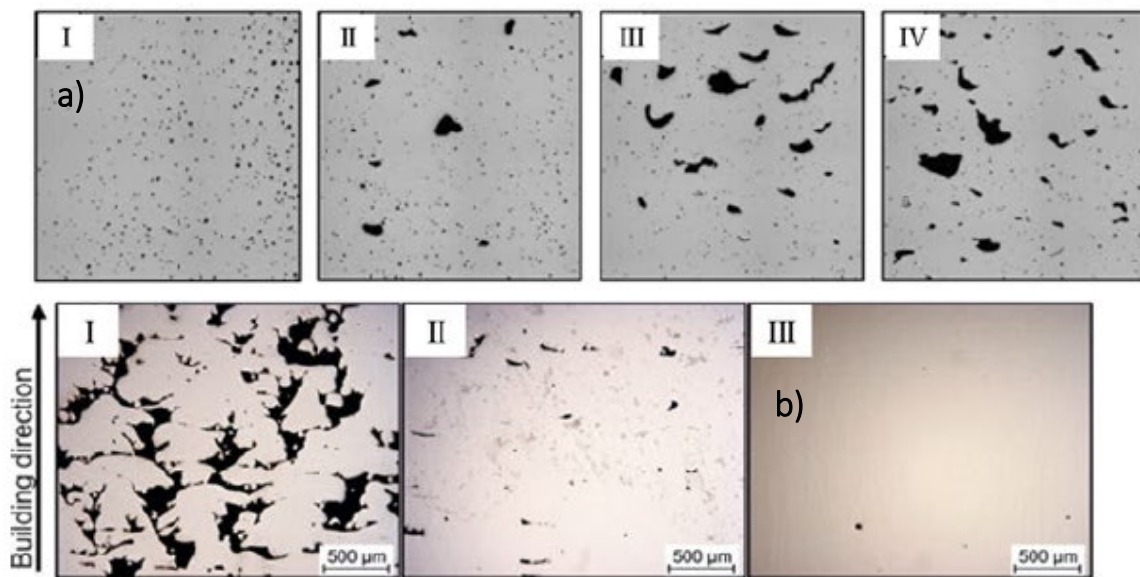


Figure 2.7 (a) Porosity effected by printing speed (I) 250 (II) 500 (III) 750 and (IV) 1000 mm/s [26], (b) Porosity effected by laser power (I) 90 (II) 120 and (III)180 W [27]

2.3.2.2 Surface Roughness

Printed components from additive manufacturing are bound to be produced with rough surfaces. As layer thickness increases, the surface roughness increases with it. Although common, rough surfaces need to be resolved since they will reduce the strength of the printed part. The rough surfaces stem from inadequate melting and balling. Inadequate melting can occur when the laser produces too little heat to completely fuse the metal powder. What is typically left is a powder particle fused to a solid surface. For the balling phenomenon to occur, the print speed is set too high. This high print speed causes balls of the particles to form at the edge of the solidified path that the laser left behind. These small balls of metal form because of the Rayleigh Instability, a phenomenon where liquids break up into smaller parts, which occurs during the metal's liquid phase [25]. Figure 2.8 demonstrates surface roughness as caused by inadequate melting and balling.

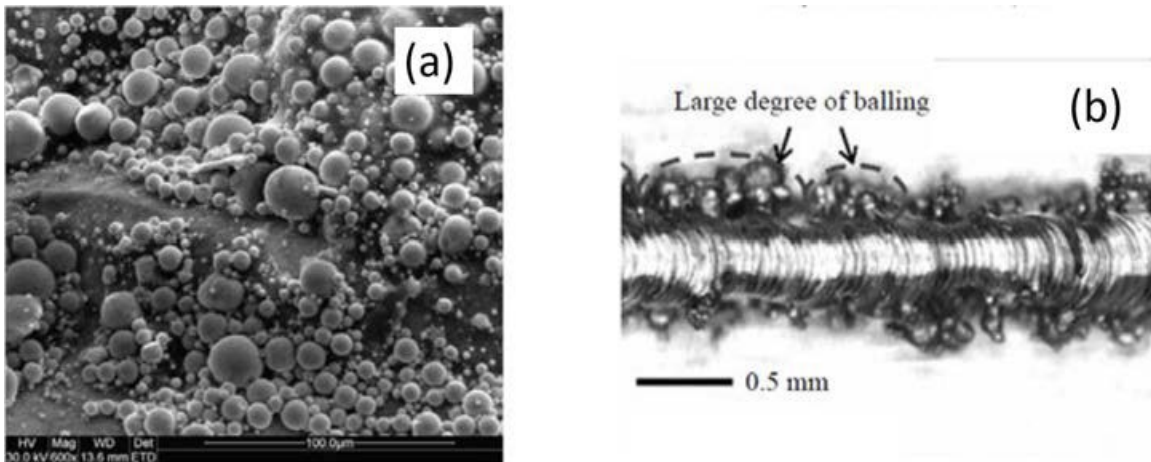


Figure 2.8 (a) SEM image of solid powders on build surface [28], (b) balling effect [29]

2.3.2.3 Cracking

In additive manufacturing parts, solidification cracking, liquidation cracking, and delamination can occur. Solidification cracking typically appears along the grain boundaries of a part. The cause of solidification cracking is the stress from the solidifying powder layer. The difference in temperatures between the layers causes this stress, and if the stress is higher than the strength of the solidifying metal, cracking will occur. In the partially melted zones, liquidation cracking can occur. This cracking appears when solidification shrinkage in the partially melted zones cause a tensile force. The force from this phenomenon causes the cracking. For delamination to occur, the yield strength of the metal must be less than the residual stress. When this happens, layers become separated since the layers are not fused [25].

2.3.3 Resolving Additive Manufacturing Limitations

Given the limitations that metallic additive manufacturing inherently comes with, there are multiple methods in overcoming these shortfalls. Porosity may not be totally unavoidable, but it can be minimized. Post processing methods such as hot isostatic pressing can internally close the pores. This method, however, is both expensive and time consuming [25]. From Figure 2.8, a slower printing speed with a higher laser power can minimize the porosity in the alloy. Surface roughness can be resolved by machining or etching the alloy until it is smooth, but it becomes impractical and difficult for complex shapes and parts where surface roughness can exist internally.

The strength of the material produced is significantly affected by porosity and rough surfaces, but heat treatment can be a solution to make up for this loss. In some

research on other alloys, such as titanium and aluminum, the temperature and length of time of the heat treatment can heavily influence the properties of the alloy. In most cases, heat treatment improved the strength of the material as well as decreased hardness [30] [31]. Even though heat treatment has no quantifiable effect on reducing pore size, it does influence an alloy's microstructure and hardness [32].

2.4 Summary

This research will investigate the properties of 70Mo-25W-5Re alloys produced through additive manufacturing. Properties such as stress, strain, porosity count, and hardness are evaluated. There is plenty of research and evaluations on Mo-W and W-Re alloys. However, little research has been conducted on this specific alloy, and there are promises of this alloy having physical properties that are useful for air and space applications. Additive manufacturing has the potential to be more beneficial than traditional tungsten and molybdenum metallurgy given how easy, quickly, and cost effective it is to produce an alloy. If the additively manufactured alloy proves to be on par with other alloys used for air and space applications, it has the potential for saving time and cost in the production of specific tungsten alloyed parts.

III. Methodology

3.1 Printing Process

The additive manufacturing equipment used to produce the samples studied in this research is the GE Additive/Concept Laser MLab 200R Cusing(R) as seen in Figure 3.1. This machine has a 100 x 100 x 100 mm build envelope with a focus diameter of approximately 50 μm and a maximum build speed of 7 m/s. This machine is also capable of accepting gases such as argon and nitrogen, which can be used during the printing process.



Figure 3.1 GE Additive/Concept Laser MLab 200R Cusing(R) [33]

The printing process involves the mixing of molybdenum, tungsten, and rhenium powders where the result is a 70% composition of molybdenum, 25% composition of tungsten, and 5% composition of rhenium. Another set of samples, studied in a parallel research effort, involves a composition of 70% molybdenum and 30% tungsten (Mo-30W). The Mo-30W samples are not the subject of this research but outcomes from that effort influenced experiment design for this research. The conditions of interest when printing the samples focuses on these main factors: the gas it was printed with and the speed the samples were printed. The conditions in which these samples were printed include a set of samples printed under argon gas and a set of samples printed with argon-3% hydrogen gas. The Mo-30W samples were printed with both argon-hydrogen and argon gas while the molybdenum, tungsten, rhenium samples were only printed in argon gas. The speed in which these samples were printed include 100 mm/s, 200 mm/s, 225 mm/s, 400 mm/s, 600 mm/s, and 800 mm/s. These samples were printed with 50 micron hatch spacing and 20 micron layer thickness. Two types of samples were printed under this print speed, and they were vertical bars and 45-degree bars as seen in Figure 3.2. These bars were roughly 18 mm long with a width of approximately 4 mm and thickness of 2 mm.



Figure 3.2 Printed 70% Mo 25% W 5% Re vertical sample (left) and 45° sample (right)

After understanding the characteristics of a broad range of printing speeds, the focus then shifted to comparing samples at 100 mm/s, 200 mm/s, 300 mm/s and 400 mm/s. Samples of these different printing speed also underwent heat treatment This step was added to understand the effect heat treatment made on the sample's microstructure. These samples were then heat treated at a temperature of 1600 °C for 4, 8, 12, and 24 hours. Another set of samples were heat treated at 2000 °C for 12 hours and 2200 °C for 6 hours.

3.2 Bend Test Preparation

Prior to the bend test, the samples must be ground to remove the residual powder that remains from the printing process. This is done to understand the strength and strain of the alloy that has been purely bonded together. Performing a bend test of a non-ground

sample will consider the strength of unbonded metal powders. To focus on the properties of the fused powder, the length of the samples must be ground off.

The samples are ground using the Buehler Ecomet 300 Grinder and Polisher (Figure 3.3) with a rotational setting of 260 revolutions per minute (rpm). The sandpaper used to grind the samples is a 240-grit silicon carbide (SiC) sandpaper. While the machine runs, the samples are applied to the surface of the sandpaper by manually applying force. Once the surface of the sample is smooth, it is washed with isopropyl alcohol and dried with nitrogen gas. The result of the grinding procedure can be seen in Figure 3.4.



Figure 3.3 Buehler Ecomet 300 Grinder and Polisher [34]

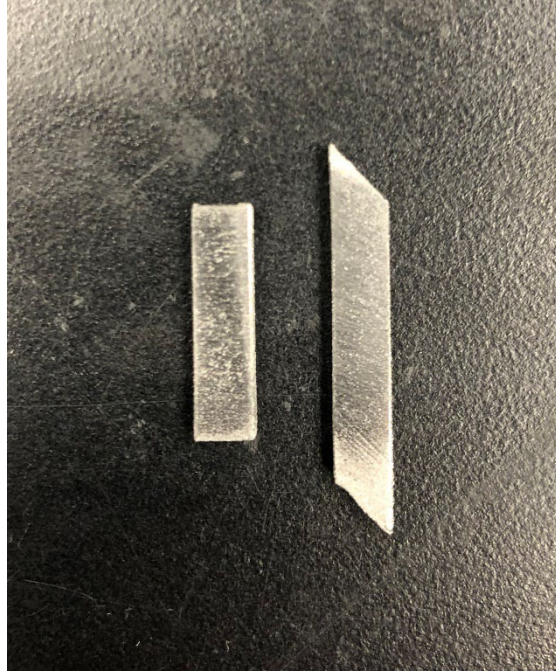


Figure 3.4 Ground 70% Mo 25% W 5% Re vertical sample (left) and 45° sample (right)

The final step prior to the bend test is all samples are baked with the OmegaLux LMF 3550 Benchtop Muffler Furnace as seen in Figure 3.5. These samples are baked for 1 hour at a temperature of 120°C. This is done so that all liquids that are left from the grinding operation are evaporated. By the end of the baking process, the samples are free of effects from residual water and alcohol.

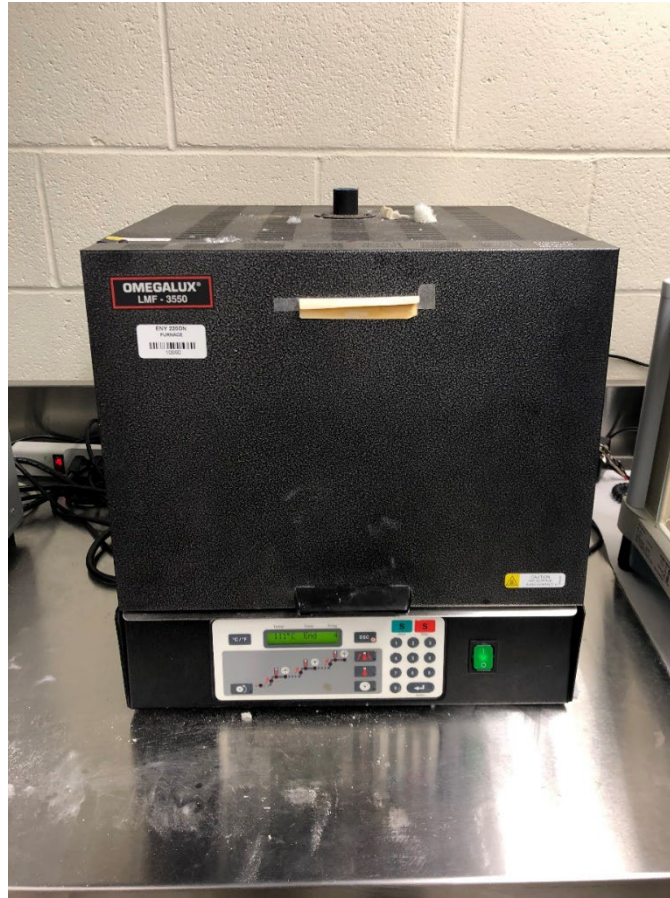


Figure 3.5 OmegaLux LMF 3550 Benchtop Muffler Furnace [35]

3.3 Bend Test Procedure

After the samples' length, width, and thickness are measured, the bend test is conducted. This test is conducted with the MTS Acumen Electromechanical Test System as seen in Figure 3.6. The samples are bent by a three-point contact process. The sample is set onto the machine by lying flat on two points. The separation between these two points is 14 mm. The third point is then applied to the top surface of the sample. This point will lightly touch the sample, and the axial distance of this point also gets recorded. Once the machine runs, the third point slowly applies an axial force on the sample. This

point continues to apply force until the sample breaks. The recorded data from this machine includes the axial displacement, axial force, and time it took for the machine to run.



Figure 3.6 MTS Acumen Electromechanical Test System [36]

3.4 Data processing

The output data of the bend test machine gives the axial displacement of the sample (in mm), the axial force applied to the sample (in kN), and the time it took for the machine to run (in seconds). Using this data and the samples' measurements, the samples' bending stress (Equation 3.1) and strain (Equation 3.2) can be determined. The breaking stress (in MPa) is calculated by the following equation:

$$\sigma = \frac{3FL}{2wt^2} \quad (3.1)$$

where, F is the axial force (in kN), L is the length between out contact points (in mm), w is the width of the sample (in mm), and t is its thickness of the sample (in mm). The bending strain is calculated by the equation:

$$\varepsilon = \frac{6Dt}{L^2} \quad (3.2)$$

where D is the axial displacement (in mm) recorded by the MTS machine. From these two formulas, the MATLAB code will calculate the stress and strain of each sample as well as the average strength and strain at fracture of each sample condition based on printing speed and heat treatment time.

3.5 Carbon Puck

Some samples after the bend test are mounted in a carbon metallographic puck. The purpose of doing this allows observation of the sample's cross-sectional surface. Analysis such as a hardness test and pore count can be done once these pucks are ground out to a smooth surface. The set up for this involves applying the broken samples into the

puck machine and applying carbon powder into the machine. The machine used to mount the samples into the carbon puck is the MetLab Metpress A as seen in Figure 3.7. This machine uses electrohydraulic pressure and heat to solidify the carbon powder with the test samples into a single uniform mold. The result after the machine runs is a mold of the carbon and samples in the shape of a puck as seen in Figure 3.8.



Figure 3.7 MetLab Metpress A [37]

Once the puck is made, the next step is to grind it. This is done in order to minimize scratches. Minimizing scratches is important because it allows some equipment to focus on the pores of the cross-sectional area. Using the grinding machine from Figure 3.3, the machine is set to 200 rpm for 1 minute. This time, grinding is accomplished with the machine rather than manually. The puck is gradually sanded with increasing grit counts, rinsed with alcohol, and dried with nitrogen gas until the scratches are minimized.

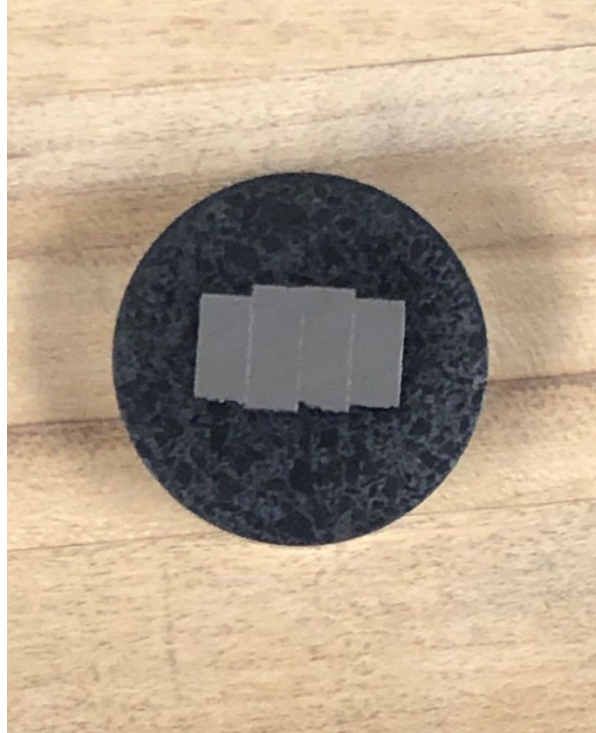


Figure 3.8 Carbon Puck

3.6 Data Analysis

Data such as fracture observations, hardness, porosity, and homogeneity are obtained using different equipment and software.

3.6.1 Fracture Surface Observations

Observations of fracture surfaces are conducted using the scanning electron microscope. Specifically, the Tescan Maia3 SEM shown in Figure 3.9 is used to capture images of the sample fracture surfaces. Samples are inserted in the machine and put in a vacuum environment. Through different settings, fracture surfaces can be imaged at large magnifications. The field views that are taken in this research vary in the micrometer scale.

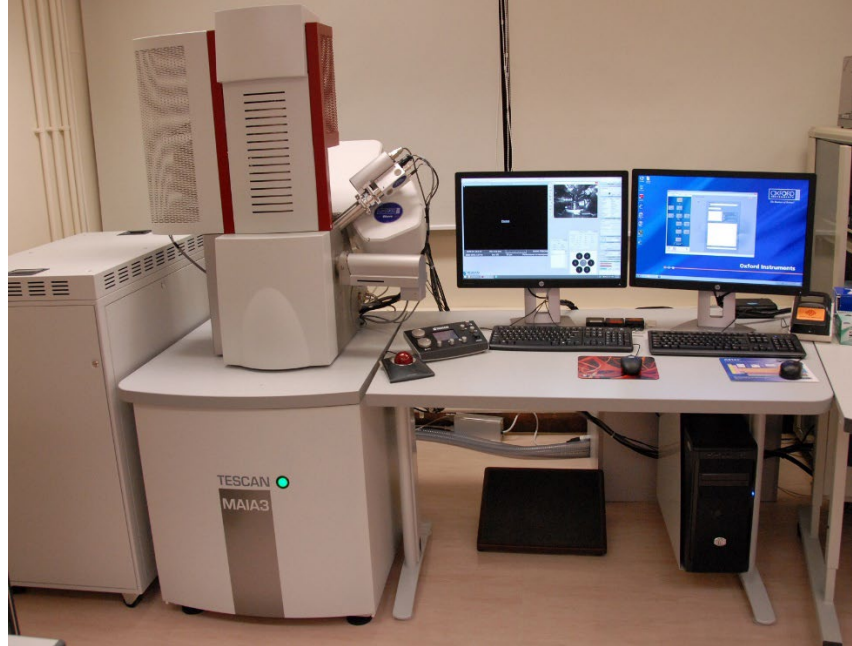


Figure 3.9 Tescan Maia3 Scanning Electron Microscope [38]

3.6.2 Hardness Testing

The hardness testing of the printed samples is conducted through the Vickers hardness test. This widely used method of testing involves using a diamond indenter with the shape of a 136° pyramid. This diamond applies a user inputted load to the surface. What is left is a square indent that is measured, and that measurement determines a unitless hardness value. The hardness value can be determined through equation 3.3 where P is the force applied and d is the length of imprint left by the indenter [39].

$$HV = 1.8544 \frac{P}{d^2} \quad (3.3)$$

The machine used to find each sample's hardness is the QATM Qness Hardness Tester as seen Figure 3.10. The settings applied on this equipment are 1 kg loads with 10 indents on specimens printed at 100 mm/s.



Figure 3.10 QATM Qness Hardness Tester [40]

3.6.3 Porosity Data

Factors such as entrapped gas and fast printing speeds can contribute to the porosity of a sample. To evaluate the porosity present in each sample, the carbon puck must have a smooth surface so that scratches are not mistaken as pores. Images of these surfaces are then taken with the Axiocam 503 mono camera and put through the Zeiss software. This software takes an image of the sample's surface and counts the number of pores in the sample and the total area of the combined pores.

3.6.4 Homogeneity Analysis

From looking at the energy dispersive x-ray spectroscopy (EDS) result, one can have a better understanding on how well each element of the alloy has mixed with each other. EDS works by taking advantage of each element's unique atomic structure. An electron gun is used to excite the elements which leads to these elements emitting x-rays. These x-rays are measured and compiled to produce a spectrum of different wavelength peaks which are used to identify different elements. The software used for EDS is conducted on the EDAX team software using a standard quality scan with a working distance of 10 mm, a magnification of 250x, and a 256x200 resolution.

IV. Analysis and Results

The first examination that will take place is the analysis of the bend test. After taking the axial force, axial displacement, and dimensions of the sample and processing the data, the breaking stress versus the percent strain can be produced. This data is useful in discovering how different printing conditions effect the samples strength and ductility. Next, the microstructure of the bent samples is observed through the scanning electron microscope. This observation can provide insight into what caused each sample to fracture as well as what possible physical trends are present at strength and strain failure. The hardness testing, porosity analysis, and homogeneity analysis are also conducted to provide insight on the alloy's internal structural properties.

4.1 Bend Test Results

The initial experiment looks at minimizing the oxygen content during the printing process. This is from the fact that oxygen has a negative influence in the grain boundaries as well as causing porosity [8]. In order to minimize oxygen, the printing process introduces two gaseous atmospheres: argon and argon-hydrogen. A comparison of the overall strength and percent strain at fracture of the samples built in these two atmospheres is shown in Figure 4.1.

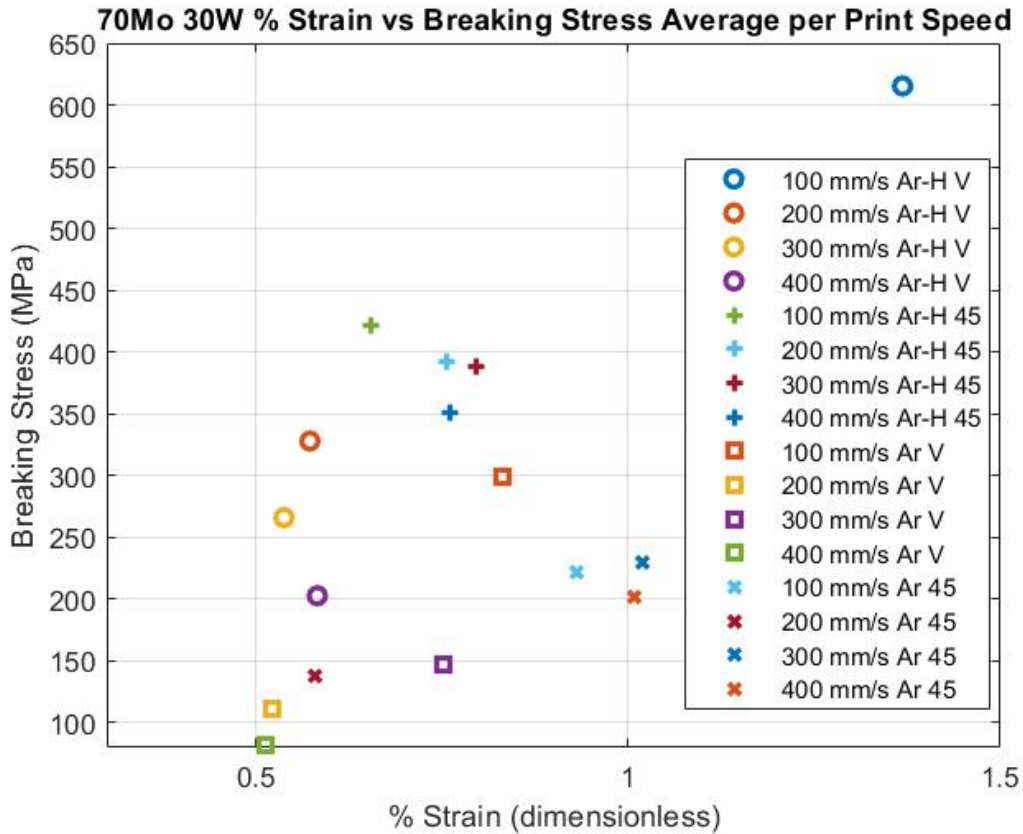


Figure 4.1 Average % Strain vs Breaking Stress per Print Speed of 70% Mo 30% W under Argon-Hydrogen and Argon Gas

From the results, the samples printed in the argon hydrogen gas outperformed the samples printed in argon gas. This could be from the argon hydrogen environment performing better with mitigating the oxygen content compared to the argon environment. Another interesting comparison to look at is the printing speeds. The results can be seen in Table 4.1.

Table 4.1 Average Breaking Stress (MPa) vs % Strain for 70% Mo 30% W

	Argon-Hydrogen Vertical Average				Argon-Hydrogen 45 Average			
Speed (mm/s)	Stress		Strain		Stress (MPa)	Stress SD	Strain	Strain SD
	Stress (MPa)	SD	Strain	SD				
100	615.34	*	1.37	*	421.82	11.36	0.65	0.05
200	328.05	21.36	0.57	0.05	392.21	11.46	0.76	0.02
300	266.00	*	0.54	*	387.68	36.47	0.80	0.04
400	202.85	11.46	0.58	0.02	350.71	8.51	0.76	0.03

	Argon Vertical Average				Argon 45 Average			
Speed (mm/s)	Stress		Strain		Stress (MPa)	Stress SD	Strain	Strain SD
	Stress (MPa)	SD	Strain	SD				
100	299.58	48.59	0.83	0.09	222.33	10.82	0.93	0.10
200	111.82	19.33	0.52	0.06	137.97	18.48	0.58	0.14
300	147.36	*	0.75	*	229.56	*	1.02	*
400	81.61	3.03	0.51	0.07	202.07	11.11	1.01	0.10

* Indicates insufficient number of samples to generate standard deviation

From observing the samples of both vertical and 45-degree samples, the results clearly shows that the slower printing speeds outperforms the faster speeds. With a slower printing speed, there is more time for the metal powders to diffuse in their molten state and form a homogeneous mixture. Better mixing and homogeneity will result in a more consistent microstructure which eliminates weak points of discontinuities of strength and ductility in the microstructure.

These previous results all came from a mixture of 70% molybdenum and 30% tungsten. The next alloy that is to be analyzed is the 70% molybdenum, 25% tungsten, and 5% rhenium alloy. For this print, the samples are printed primarily through an argon-hydrogen atmosphere since it produced better strength and percent strain results. The results of the breaking stress vs percent strain of all samples can be seen in Figure 4.2. Figure 4.3 and Table 4.2 features the average breaking stress vs percent strain of each printing speed.

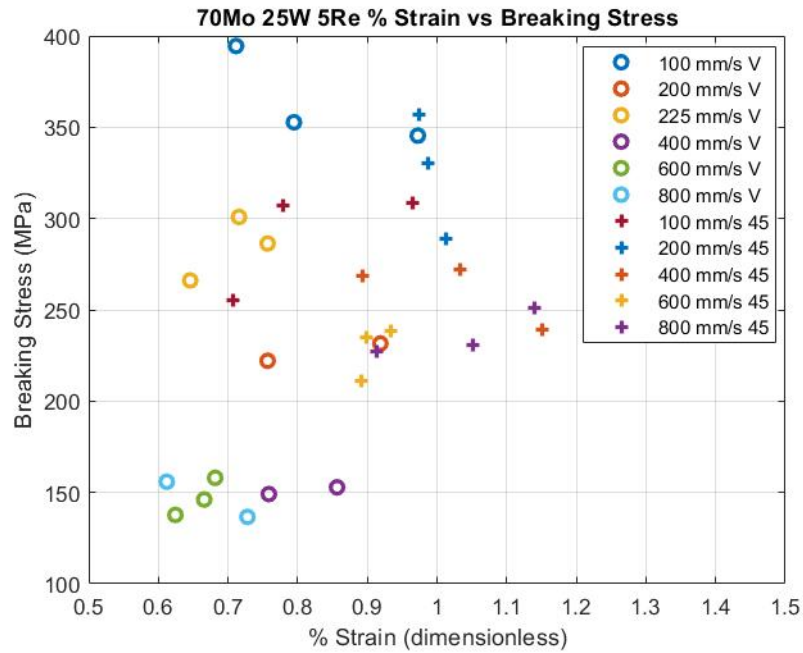


Figure 4.2 % Strain vs Breaking Stress of 70% Mo 25% W 5% Re

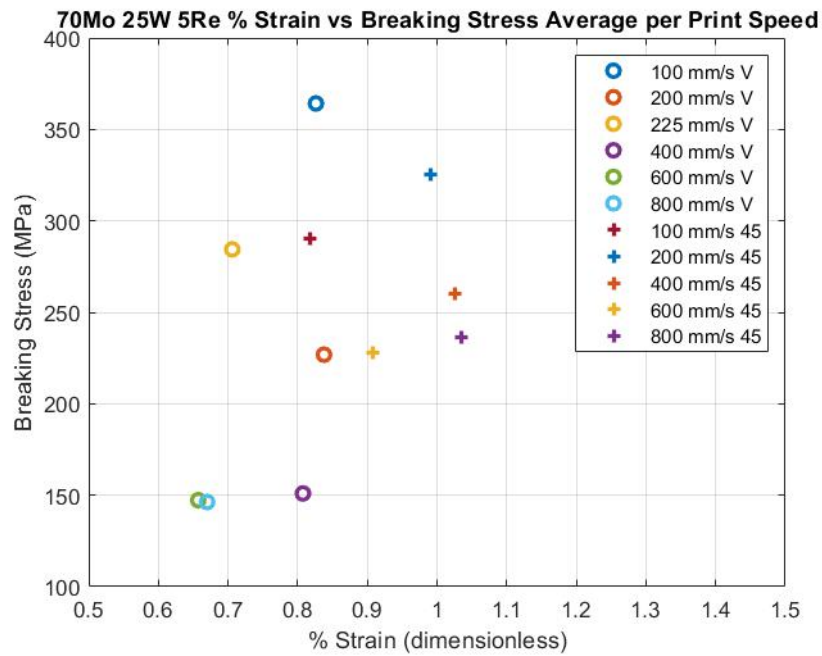


Figure 4.3 Average % Strain vs Breaking Stress per Print Speed of 70% Mo 25% W 5% Re

Table 4.2 Average Breaking Stress (MPa) vs % Strain of 70% Mo 25% W 5% Re

Speed (mm/s)	Non Heat Treated Vertical Average				Non Heat Treated 45 Average			
	Stress (MPa)	Stress SD	Strain	Strain SD	Stress (MPa)	Stress SD	Strain	Strain SD
100	364.205	21.616	0.826	0.109	290.238	24.868	0.817	0.109
200	226.832	*	0.838	*	325.303	27.992	0.991	0.016
225	284.430	14.244	0.706	0.046				
400	150.947	*	0.808	*	259.972	14.798	1.026	0.106
600	147.272	8.331	0.657	0.024	228.228	12.166	0.908	0.019
800	146.252	*	0.670	*	236.370	10.362	1.035	0.093

* Indicates insufficient number of samples to generate standard deviation

From comparing the two alloys printed in argon-hydrogen, the 70% Mo 25% W 5% Re alloy has a lower breaking stress value than the 70% Mo 30% W alloy when comparing by printing speed. Apart from the 70% Mo 30% W printed at 100 mm/s, the overall ductility of the 70% Mo 25% W 5% Re alloy is higher. This could be due to the difference in homogenous microstructure. The 70% Mo 30% W alloy printed at 100 mm/s has a more consistent stress strain response, meaning there are less weak spots to weaken it. The difference in strength between the two types of alloys could be from the difference in the alloy's metallic mixture. Rhenium is generally lower in tensile and yield strength than tungsten. By removing some tungsten and replacing it with rhenium, there is an expectation that the strength will decrease. The breaking stress and percent strain from Table 4.2 are the properties of the sample straight out of the additive manufacturing machine. An additional heat treatment process, however, changes the composition of the sample. Figure 4.4 reveals the average breaking stress and percent strain of the 70% Mo 25% W 5% Re samples that underwent a heat treatment for 0, 4, 8, 12, and 24 hours. Table 4.3 shows the average stress and strain of the heat-treated samples per

printing speed. A comparison of the stress and strain as heat treatment time increases can be seen in Figure 4.5 and Figure 4.6 for vertical samples and Figure 4.7 and Figure 4.8 for 45-degree samples.

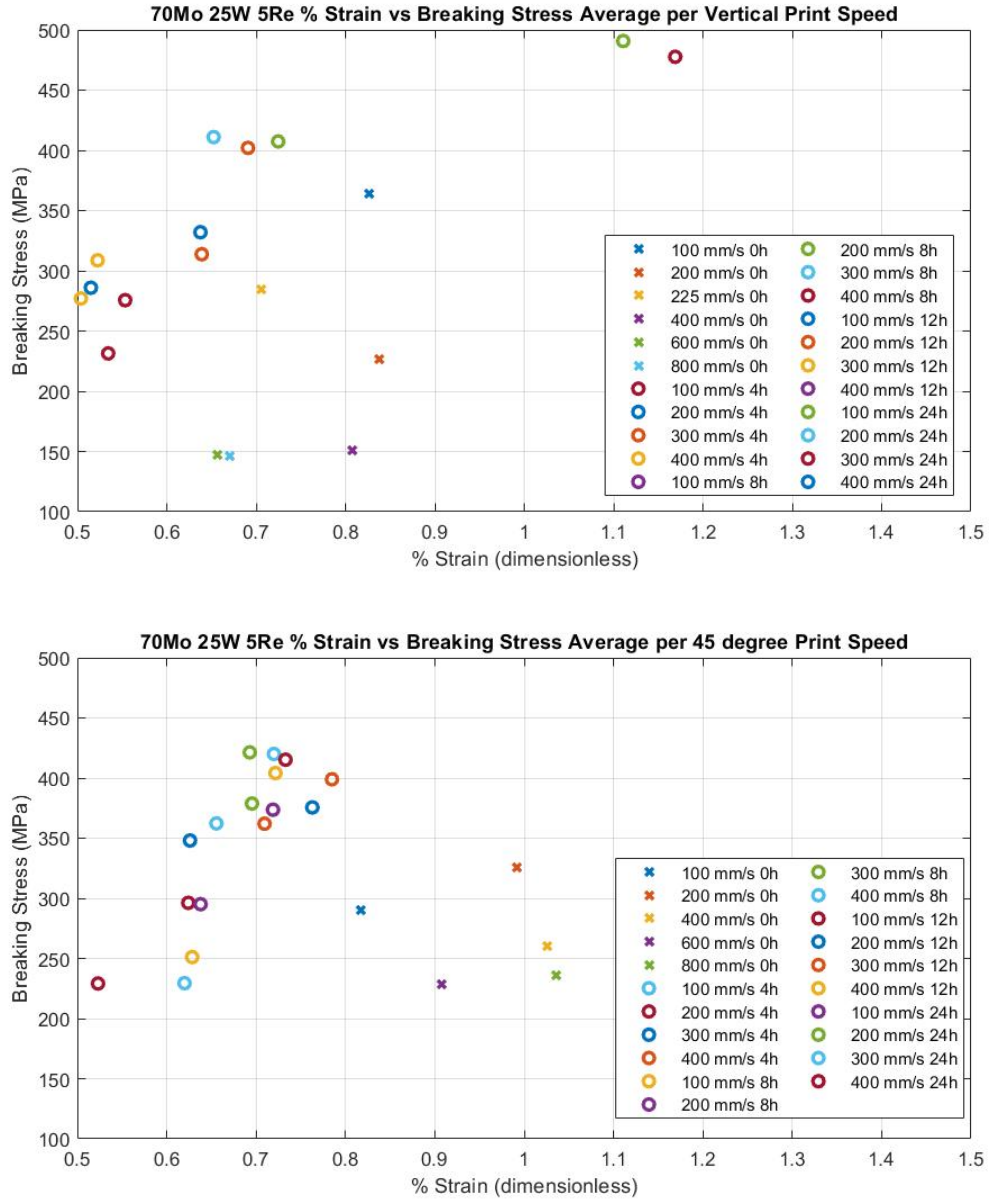


Figure 4.4 Average % Strain vs Breaking Stress per Print Speed of Heat Treated 70% Mo 25% W 5% Re

Table 4.3 Average Breaking Stress (MPa) vs % Strain of Heat Treated 70% Mo 25% W 5% Re

	4h Heat Treated Vertical Average				4h Heat Treated 45 Average			
Speed (mm/s)	Stress (MPa)	Stress SD	Strain	Strain SD	Stress (MPa)	Stress SD	Strain	Strain SD
100	477.66	13.27	1.17	0.04	229.46	82.75	0.62	0.28
200	332.03	120.34	0.64	0.13	296.25	61.52	0.62	0.13
300	313.75	16.91	0.64	0.16	348.07	15.96	0.63	0.06
400	276.99	42.97	0.50	0.10	398.99	*	0.78	*
	8h Heat Treated Vertical Average				8h Heat Treated 45 Average			
Speed (mm/s)	Stress (MPa)	Stress SD	Strain	Strain SD	Stress (MPa)	Stress SD	Strain	Strain SD
100	500.25	41.54	1.39	0.68	251.16	22.20	0.63	0.11
200	407.40	9.22	0.73	0.09	373.70	16.26	0.72	0.10
300	305.95	10.21	0.47	0.02	378.80	24.89	0.70	0.02
400	231.39	38.52	0.53	0.15	362.28	*	0.66	*
	12h Heat Treated Vertical Average				12h Heat Treated 45 Average			
Speed (mm/s)	Stress (MPa)	Stress SD	Strain	Strain SD	Stress (MPa)	Stress SD	Strain	Strain SD
100	458.69	26.41	1.62	0.18	229.17	18.68	0.52	0.04
200	402.03	37.91	0.69	0.05	375.61	11.45	0.76	0.04
300	308.71	36.20	0.52	0.07	362.06	17.20	0.71	0.05
400	237.58	5.22	0.48	0.08	404.17	6.03	0.72	0.10
	24h Heat Treated Vertical Average				24h Heat Treated 45 Average			
Speed (mm/s)	Stress (MPa)	Stress SD	Strain	Strain SD	Stress (MPa)	Stress SD	Strain	Strain SD
100	490.78	16.68	1.11	0.10	295.14	29.43	0.64	0.04
200	411.01	28.54	0.65	0.01	421.39	11.50	0.69	0.03
300	275.61	26.15	0.55	0.01	420.05	23.91	0.72	0.11
400	285.95	*	0.52	*	415.29	17.29	0.73	0.09

* Indicates insufficient number of samples to generate standard deviation

Stress vs Heat Treatment Time per Vertical Print Speed

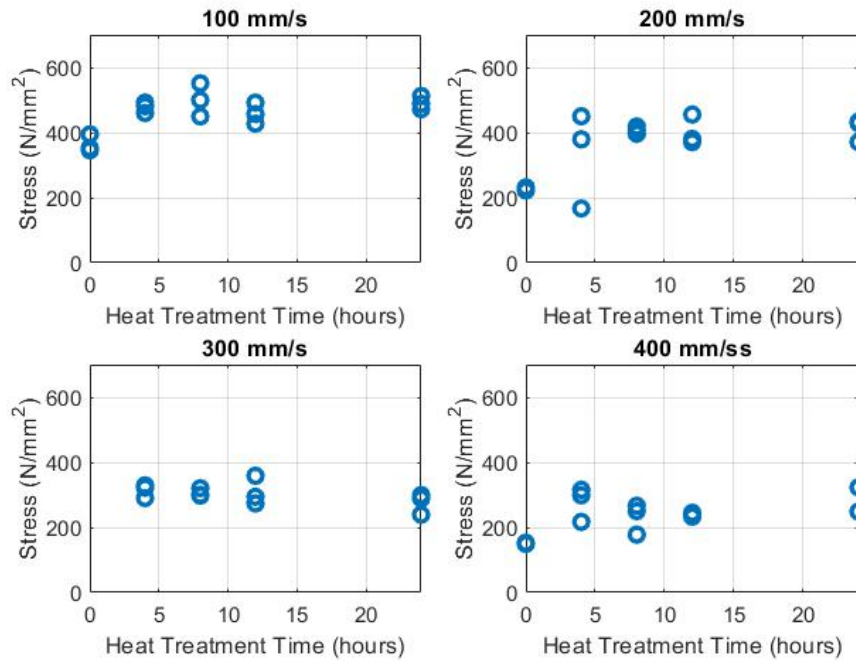


Figure 4.5 Stress vs Heat Treatment Time per vertical print speed

Strain vs Heat Treatment Time per Vertical Print Speed

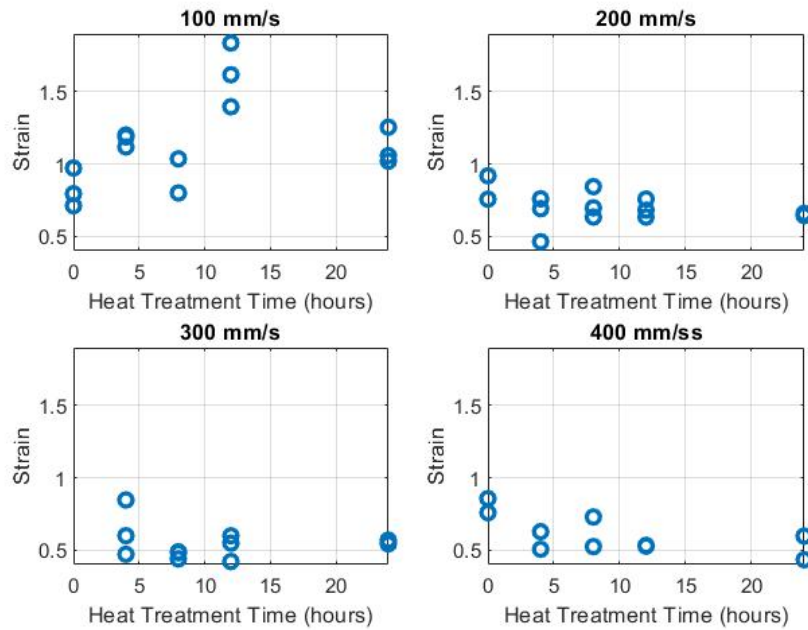


Figure 4.6 Strain vs Heat Treatment Time per vertical print speed

From just heat treating the samples for 4 hours, the stress and strain significantly improved. The average strength jumped up to an average of 100 MPa and the average percent strain improved by a factor of 0.3 in some cases. However, the average strain also drops by a factor of 0.2 in other cases. In general, the breaking strength is increased, and maximum strain decreased with longer heat treatments. An example of a significant improvement is seen comparing the 45-degree sample printed in 400 mm per second and heat treated for 24 hours (Table 4.3) with the non-heat-treated 45-degree sample printed with a speed of 100 mm per seconds (Table 4.2). The average breaking stress jumps from 290.23 MPa to 415 MPa. The only case of a sample not improving in strength is the case of a vertically 4-hour heat treated sample printed at 200 mm/s as seen in Figure 4.5. Ultimately this value caused a large standard deviation of 120 which brings down the average value of all samples in that category.

The amount of time the samples are heat treated did not have a clear correlation in affecting the strength. For example, a sample printed at 100 mm/s and heat treated for 4 hours had a similar stress and strain to another sample printed at 100 mm/s and heat treated for 8, 12, and 24 hours. Looking at the standard deviation of these same samples show that the distance from the mean is similar for 8, 12, and 24 hours while the 4-hour heat treatment sample has a much higher deviation from the mean. At minimum, heat treating the printed sample for at least 4 hours changed the strength of the material. Besides the percent strain of the 100 mm/s sample in Figure 4.6, the percent strain appears to do a slight decrease after post heat treatment.

In order to have a better understanding on the effects of heat treatment, some samples were also treated at differing temperatures. All samples heat treated at a different

temperature are printed with argon gas. Vertical and 45-degree samples are printed at 100 mm per second and 400 mm per second. The 45-degree samples and some of the vertical samples are then heat treated for 12 hours at 2000 °C. The rest of the vertical samples are heat treated for 6 hours at 2200 °C. The result of their average stress strain values can be seen in Figure 4.10 and Table 4.4. The stress strain is found in Figure 4.9. A comparison of the different heat treatment temperatures can be found in Figure 4.11, Figure 4.12, and Figure 4.13.

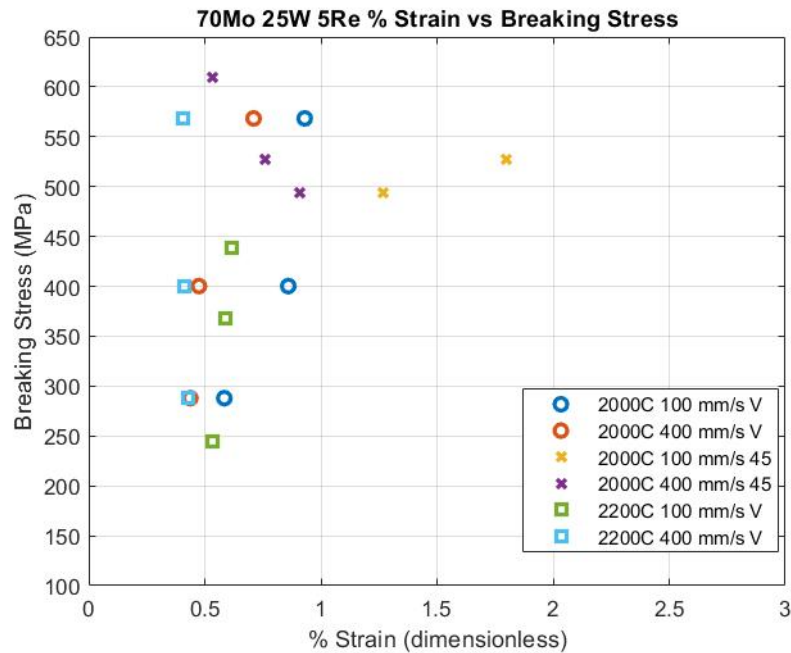


Figure 4.9 % Strain vs Breaking Stress of Heat Treated 70% Mo 25% W 5% Re at 2000 °C and 2200 °C

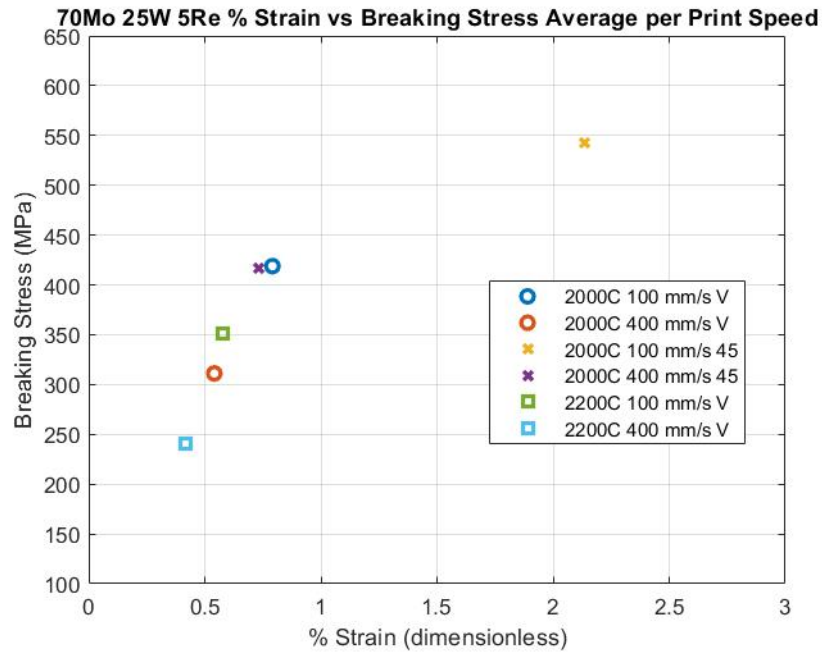


Figure 4.10 Average % Strain vs Breaking Stress per Print Speed of Heat Treated 70% Mo 25% W 5% Re at 2000 °C and 2200 °C

Table 4.4 Average Breaking Stress (MPa) vs % Strain of Heat Treated 70% Mo 25% W 5% Re

	12h Heat Treated 2000C Vertical Average				12h Heat Treated 2000C 45 Average			
Speed (mm/s)	Stress (MPa)	Stress SD	Strain	Strain SD	Stress (MPa)	Stress SD	Strain	Strain SD
100	418.87	115.23	0.79	0.15	543.33	48.47	2.14	0.88
400	311.14	43.99	0.54	0.12	417.40	162.03	0.73	0.16
	12h Heat Treated 2000C Vertical Average							
Speed (mm/s)	Stress (MPa)	Stress SD	Strain	Strain SD				
100	350.63	80.09	0.58	0.04				
400	240.90	18.97	0.41	0.01				

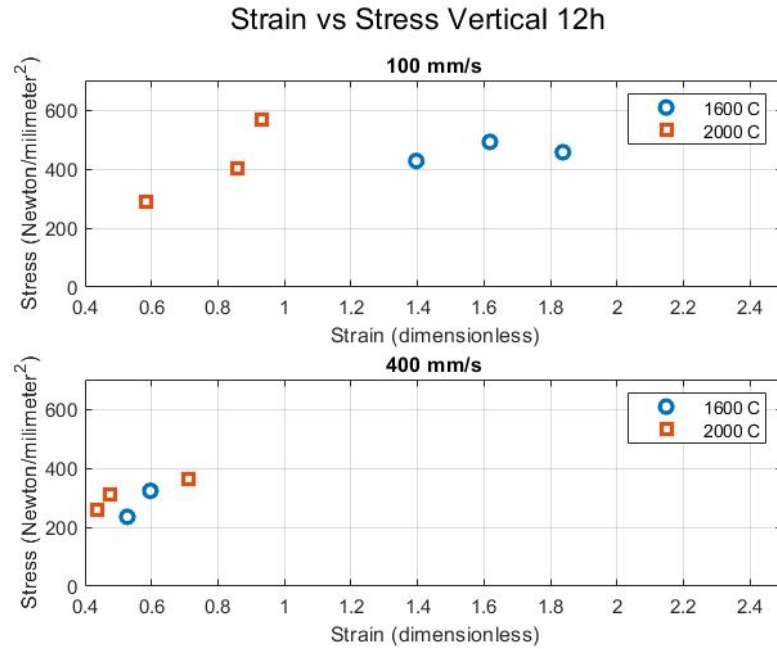


Figure 4.11 Strain vs stress for vertical samples heat treated at 1600 °C and 2000 °C

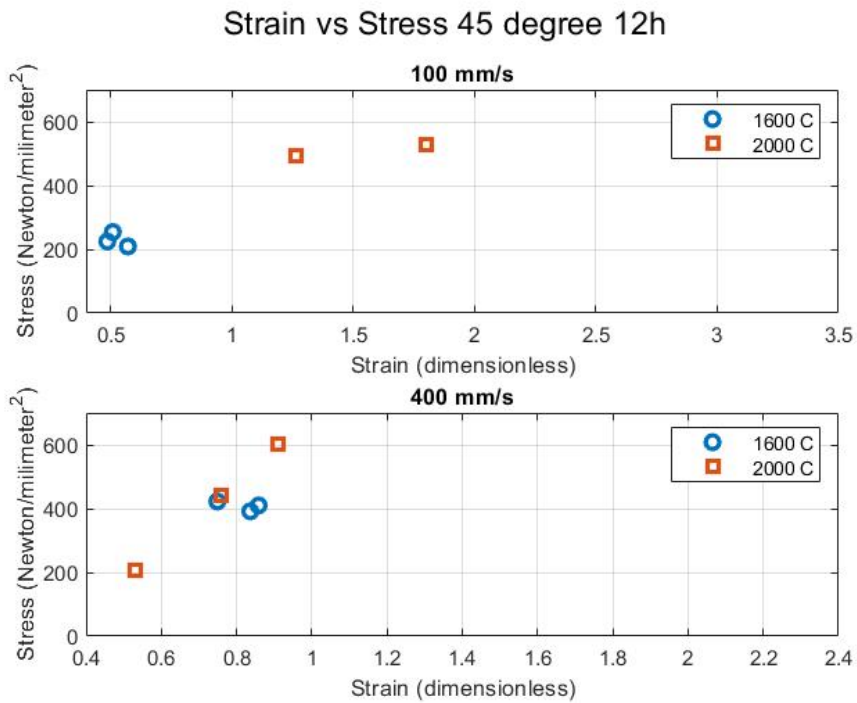


Figure 4.12 Strain vs stress for 45° samples heat treated at 1600 °C and 2000 °C

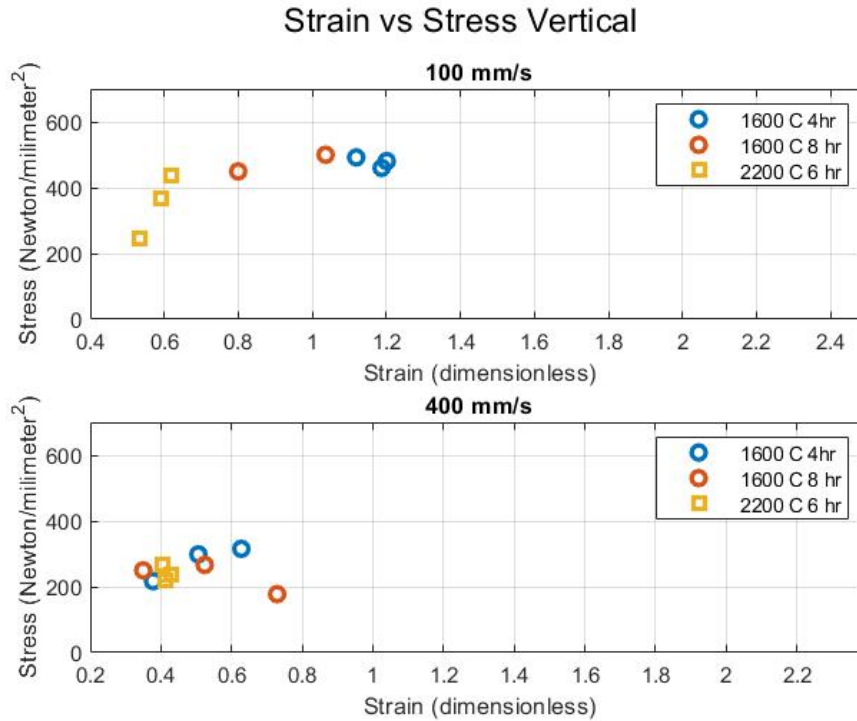


Figure 4.13 Strain vs stress for vertical samples heat treated at 1600 °C and 2200 °C

When comparing the values of samples heat treated at high temperatures with samples heat treated at a relatively lower temperature, there is a noticeable slight decrease in stress and strain value as the temperature of heat treatments go up. The only outlier is the comparison of the 45-degree samples where the stress and strain increased as the temperature went up. Considering that the samples are relatively close in stress and strain values, it is worth investigating the properties of this alloy printed with hydrogen and heat treated at these higher temperatures.

4.2 Scanning Electron Microscope (SEM) results

The SEM is used to analyze the samples at a microscopic level. At this magnitude, it becomes easier to observe the fracture surface of different materials. In this experiment, the fracture surface of the different printing speeds and heat treatments are

observed. The fracture surface of the argon sample shows evidence on the sample's weaker nature. Figure 4.14 shows a significant amount of molybdenum oxide indicated by the bright spots. This formation as discussed in Chapter 2 is known to weaken molybdenum alloys.

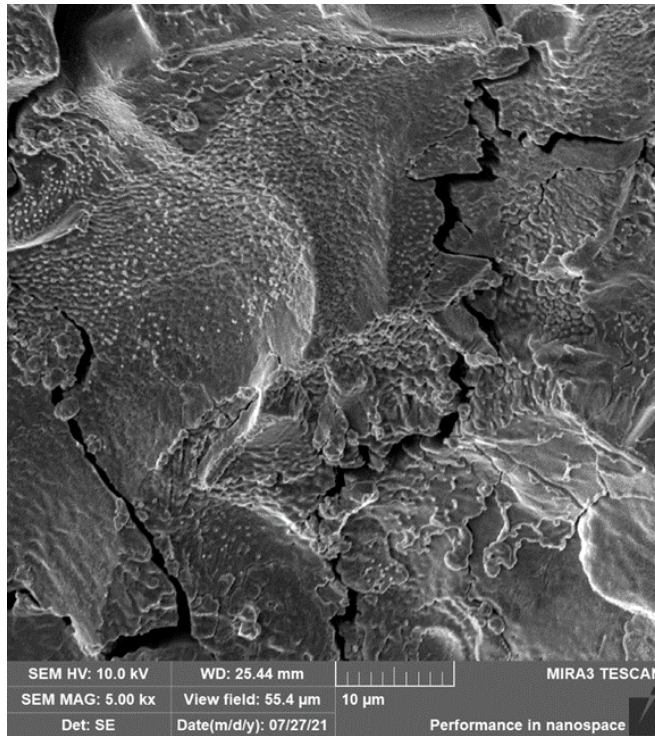


Figure 4.14 Molybdenum Oxide formed at the fracture surface

Another interesting observation is comparing surface images of samples printed at different speeds. Figure 4.15 shows the fracture surface of a non-heat-treated sample printed in both 100 mm per second and 600 mm per second.

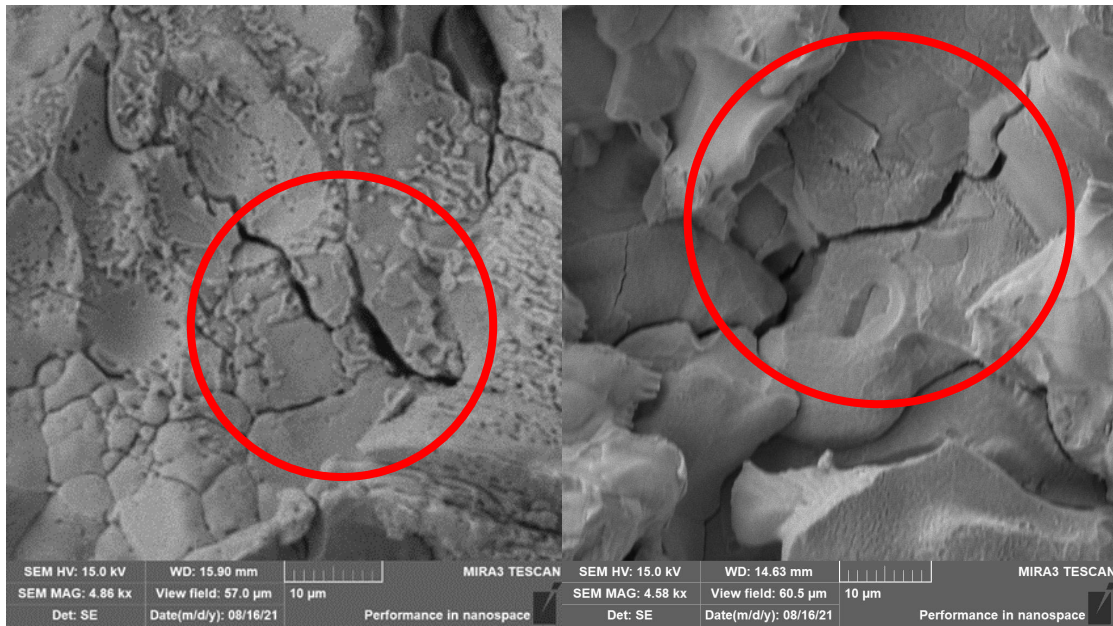


Figure 4.15 70Mo-25W-5Re fracture surface of the 100 mm/s sample (left) and the 600 mm/s sample (right) at 5.0kx magnitude highlighting different crack sizes

Both samples are made from the same mixture ratio, and both are printed from the same hydrogen batch. The difference between their creation is the printing speed. From the figure above, it is noticeable to see that the cracks are longer in the faster printing speed than the slower printing speed. A longer fracture indicates that there is some weakness in the fusing between the metal powders during the printing process. This fracture is evident that the slow printing speed leads to a greater strength and percent strain as discussed in section 4.1 and as seen in Table 4.1.

Another byproduct of a slower printing speed can be seen in Figure 4.16 where the samples are taken at a 1000x magnitude.

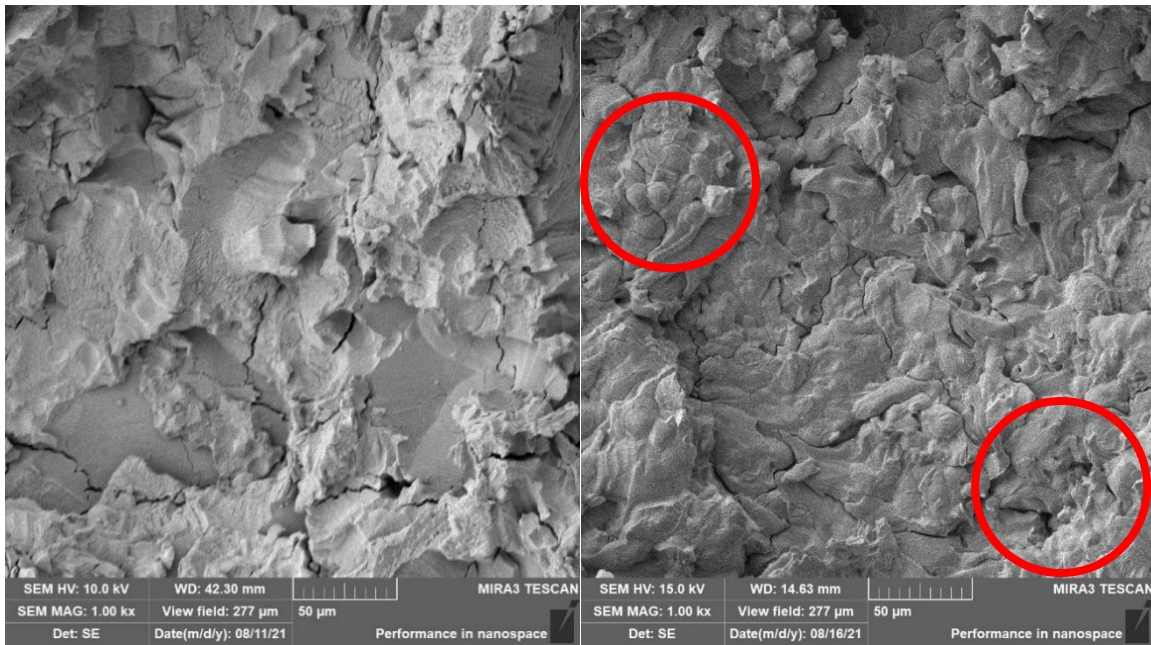


Figure 4.16 70Mo-25W-5Re fracture surface of the 100 mm/s sample (left) and the 600 mm/s sample (right) at 1.0kx magnitude highlighting unmelted particles

From the faster printing speed, the shape of the partially melted particles is more noticeable when compared to the slower printing speed. On the right side of Figure 4.16, there are some noticeable bumps and grooves that have a rounded shape. The left side of the figure has some rounded shapes as well, but not as frequent as the one on the right. With a faster printing speed, there is less time for heating leading to less time for the metallic powders to be melted together. What is left is a product of partially melted particles which significantly affect the homogeneity and therefore the strength of the material as noted from Table 4.2 from section 4.1.

As mentioned in section 4.1, the amount of time a sample is heat treated did not significantly affect the strength. Through SEM observations, the fracture surfaces are similar across samples with similar printing speeds despite being heat treated for a different amount of time. Like the non-heat-treated samples, the printing speed played a

bigger factor in strength, and it can be seen through the size of the cracks and number of particles left unmelted. Samples such as the ones seen in Figure 4.17 show similar features such as unmelted particles despite being heat treated at different times. These observations lead to the conclusion that 1600°C is an insufficient temperature to develop significant microstructural evolution in this alloy.

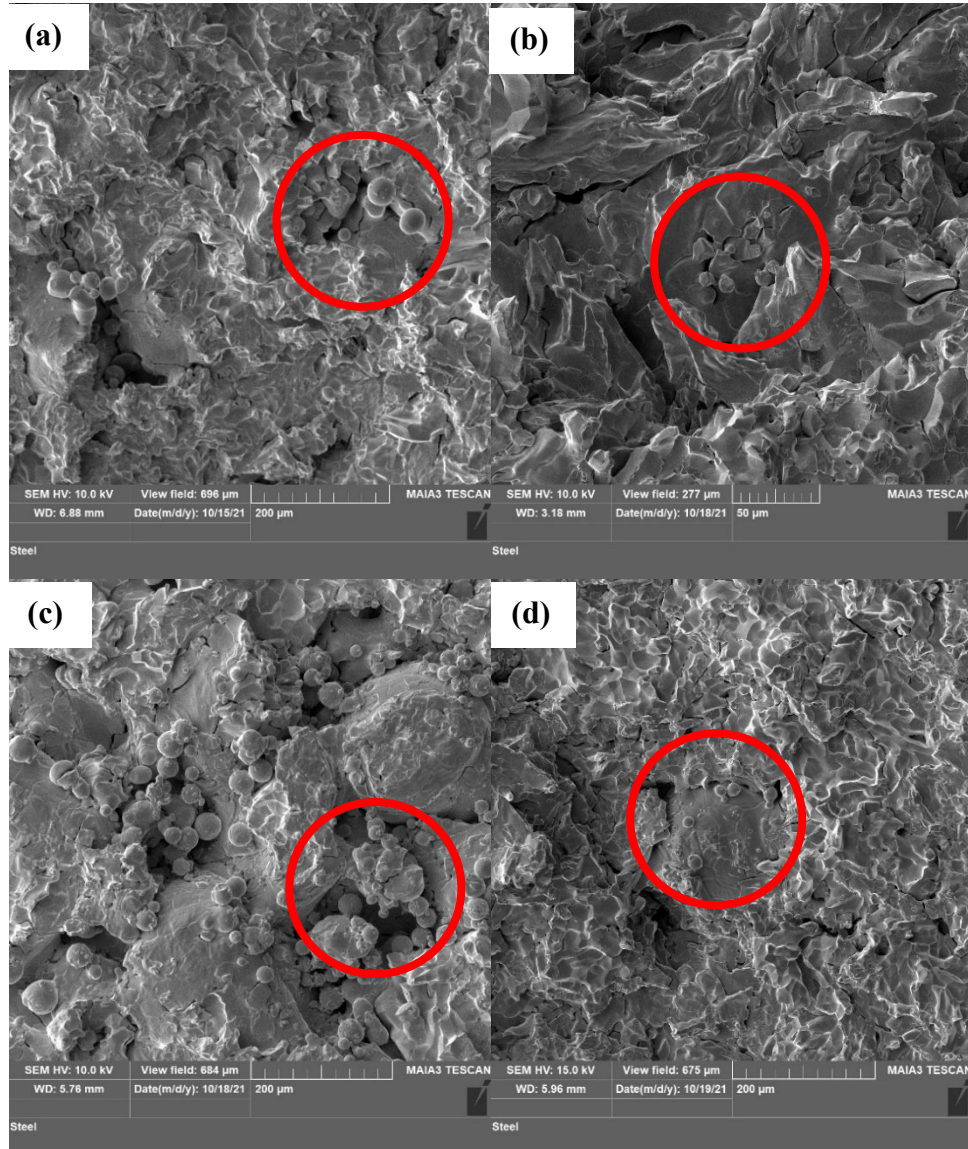


Figure 4.17 70Mo-25W-5Re fracture surface of the 300 mm/s sample heat treated at (a) 4 hours (b) 8 hours (c) 12 hours (d) 24 hours highlighting unmelted particles

4.3 Vickers Hardness Test

The Vickers Hardness test is a method in determining the hardness of a material. This measurement is determined by how much resistance a material has to deformation. The hardness test involves a machine applying pressure onto the surface of a material and applying an indentation onto the surface. The size of the indent is measured, and that measurement determines the hardness value (HV) of the material. The average hardness value for the 100 mm per second samples can be seen in Table 4.5.

Table 4.5 Average Hardness Value of various heat treated 100 mm/s samples

	Mean Value	Range	Hardness Min	Hardness Max	Standard dev.
0 hours	219.4	44	197	241	12.62
4 hours	177.3	67	137	204	18.64
8 hours	177.9	41	157	198	13.45
12 hours	174.2	23	161	184	7.04
24 hours	172	41	151	192	13.17

From the results, the hardness stayed consistent across heat treated specimens. The hardness value of the heat-treated samples stayed consistent with a value of approximately 175. The drastic change in hardness occurs when the non-heat-treated specimen goes through heat treatment. The hardness dropping from heat treatment may indicate that the temperature was sufficient to lead to recovery of the material. Recovery is a process by which strain is able to diffuse out of the crystal lattice which would impact the residual stress in the grains and give a lower value of hardness. This process described means that the 1600 °C heat treatment acted like a stress relief, but not sufficiently high to cause recrystallization or homogenization of the unmixed microstructure. Further evidence of the recovery phase can be seen in section 4.5 through

the EDS data. Homogenization is not accomplished, so the only other explanation of the lowered hardness value is recovery.

4.4 Porosity Analysis

The amount of porosity found in an additively manufactured alloy is an important factor when understanding its strength. A highly porous metal is subject to fracture when experiencing a large amount of force. Therefore, it is of interest that these metals remain dense with minimal pores in order to avoid catastrophe when it is used as a part. The porosity of the carbon pucks is first analyzed through the Axiocam 503 mono camera. Figure 4.18 shows an example of what the porosity under the microscope looks like.

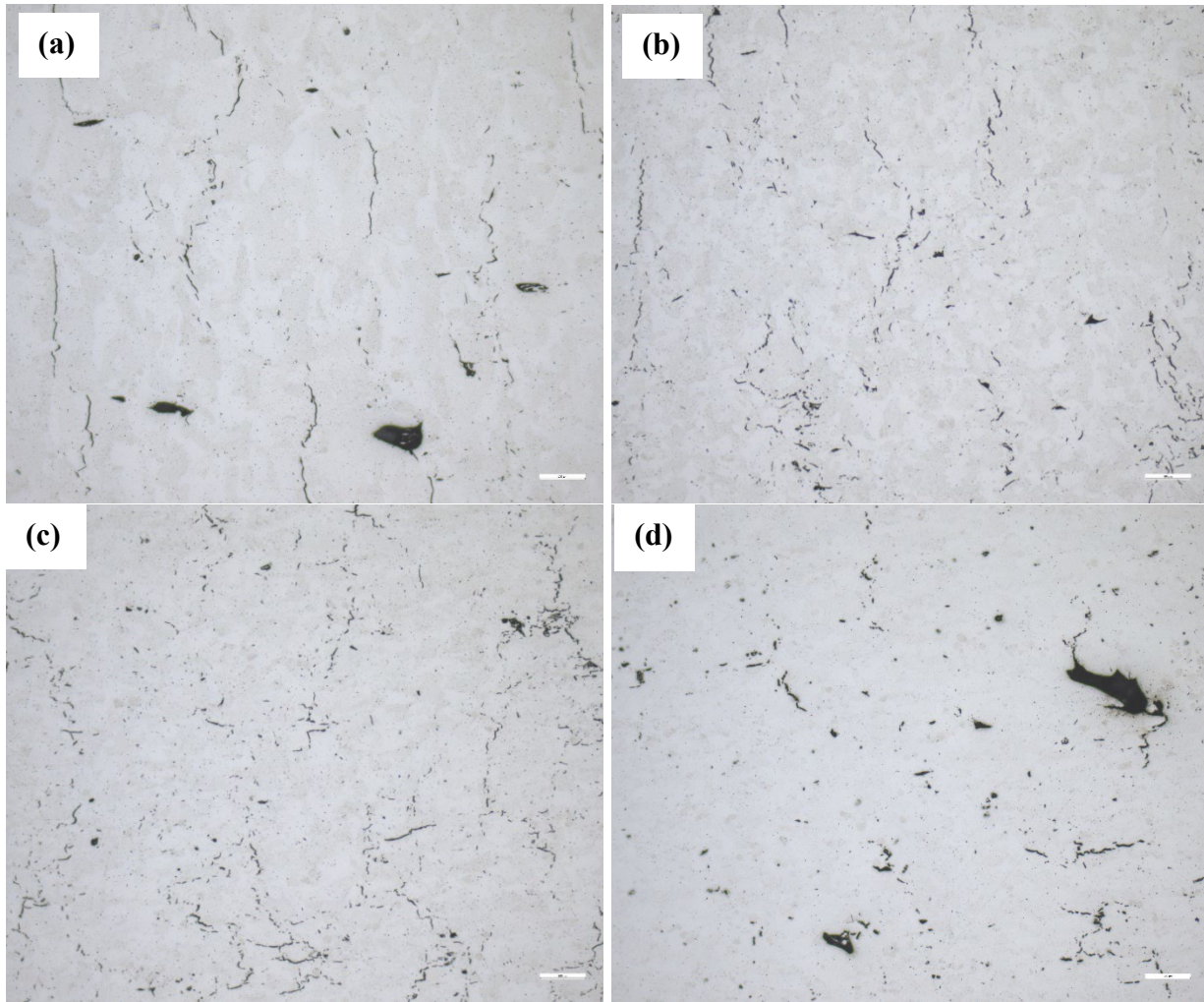


Figure 4.18 Porosity of 70Mo-25W-5Re under a 4-hour treatment with printing speeds of (a) 100 mm/s, (b) 200 mm/s, (c) 300 mm/s, (d) 400 mm/s

The Zeiss software is used to count the number of pores and measure the pore's area on the surface of the samples. Figure 4.19 shows an example of the porosity count and Table 4.6 shows the porosity count and total pores area for each heat-treated sample of differing printing speeds.

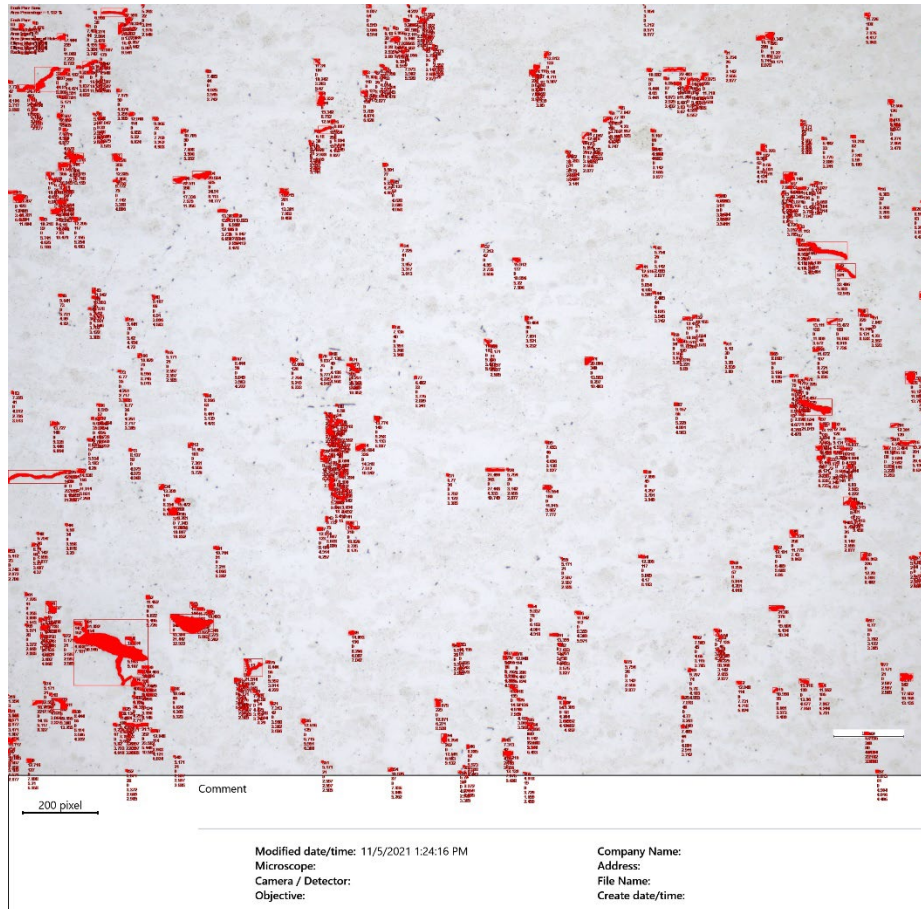


Figure 4.19 Pore count of a non-heat-treated sample printed at 100 mm per seconds

Table 4.6 Pore count and pores area size of each 70Mo-25W-5Re sample

Sample	Count #	Area	Sample	Count #	Area
0h - 100	356	1.132	12h - 100	405	1.267
0h - 200	330	1.275	12h - 200	1383	3.4
0h - 400	321	1.66	12h - 300	1388	4.33
			12h - 400	1749	6.35
4h - 100	411	2.133	24h - 100	590	1.72
4h - 200	774	2.354	24h - 200	1046	3.542
4h - 300	1181	3.576	24h - 300	1770	5.414
4h - 400	549	3.675	24h - 400	1749	4.539
8h - 100	607	1.903			
8h - 200	637	1.731			
8h - 300	1024	2.471			
8h - 400	1186	2.369			

As expected, the most noticeable factor of porosity is printing speed. As seen from Table 4.6, porosity tended to have a steady increase as the printing speed increases. When comparing the porosity results of the non-heat-treated alloys with the heat-treated alloys, it is easy to conclude that heat treatment alone does not decrease porosity. Instead, it appears to increase it. For porosity to noticeably change, pressure must also be included during the heat treatment process. Process like hot isostatic press were not conducted in this research.

4.5 Energy Dispersive X-ray Spectroscopy (EDS) results

The EDS result of the alloy shows that the overall concentration has stayed consistent with the alloy concentration of tungsten, molybdenum, and rhenium. The printing speed and length of time on heat treatment showed that the overall concentration profile of the material did not change. The concentration of molybdenum stayed roughly around 70%, but the tungsten concentration ranged from 26 to 34% while rhenium averaged less than 4% in concentration for samples heat treated at 1600 °C, 2000 °C, and

2200 °C. Table 4.7 displays the average concentration of samples printed at different speeds and heat treated at different times. Table 4.8 displays additional concentrations for different heat treatment temperatures. Figure 4.20 shows the EDS spectra of one of the samples. No other elements were detected in the spectra such as hydrogen or oxygen, but these elements can be difficult to impossible to quantify well with the process because of the nature of the technique.

Table 4.7 Average Concentration of Mo, W, and Re at different printing speeds and heat treatment time

Concentration at 1600 C				
Heat Treatment (hours)	Speed (mm/s)	Mo Average (Weight%)	W Average (Weight%)	Re Average (Weight%)
4	100	70.45	26.98	2.57
4	200	72.22	25.06	2.72
4	300	71.84	25.67	2.50
4	400	68.44	28.49	3.07
8	100	67.34	29.78	2.88
8	200	69.88	27.05	3.08
8	300	72.09	25.63	2.27
8	400	69.94	27.45	2.61
12	100	72.38	25.11	2.51
12	200	68.26	28.75	2.99
12	300	76.56	21.53	1.93
12	400	69.42	27.63	2.95
24	100	69.90	27.62	2.48
24	200	67.87	29.33	2.81
24	300	74.16	23.54	2.30
24	400	67.40	29.23	3.37

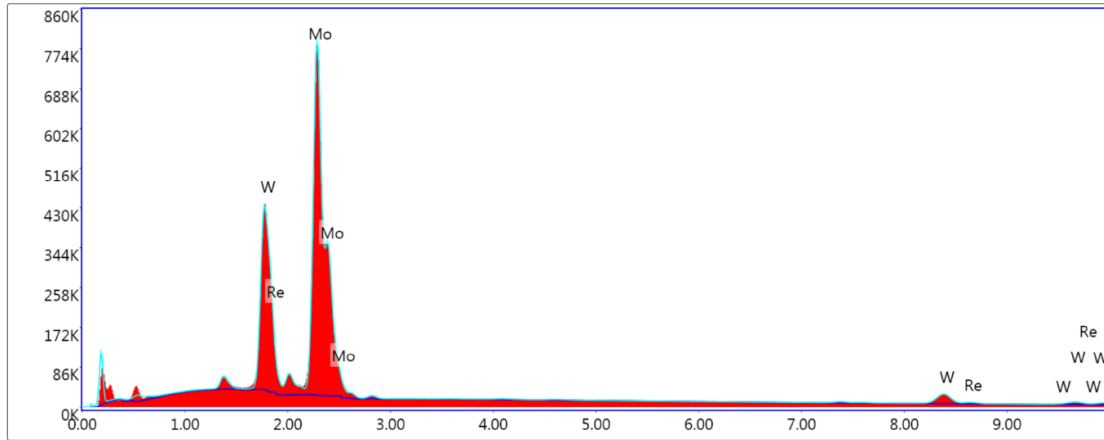
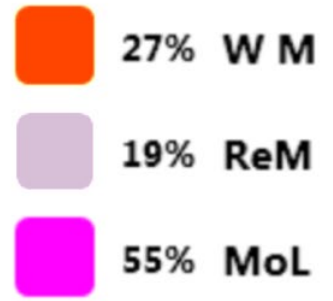
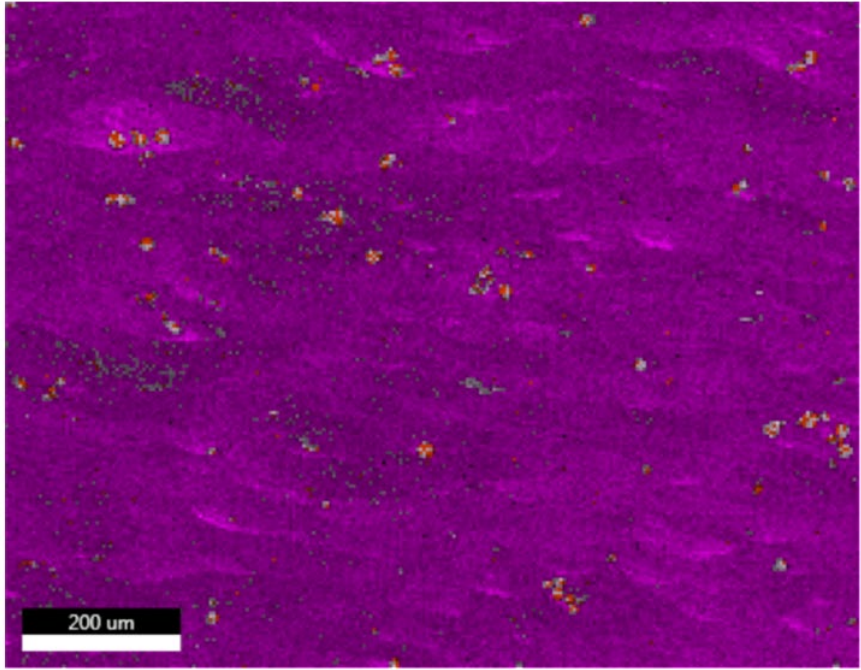


Figure 4.20 Characteristic X-ray spectrum of 70Mo-25W-5Re printed at 100 mm/s and heat treated for 4 hours

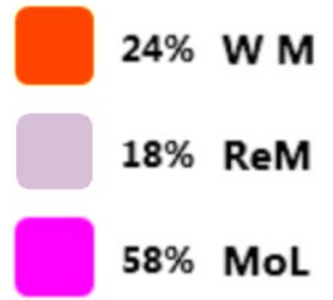
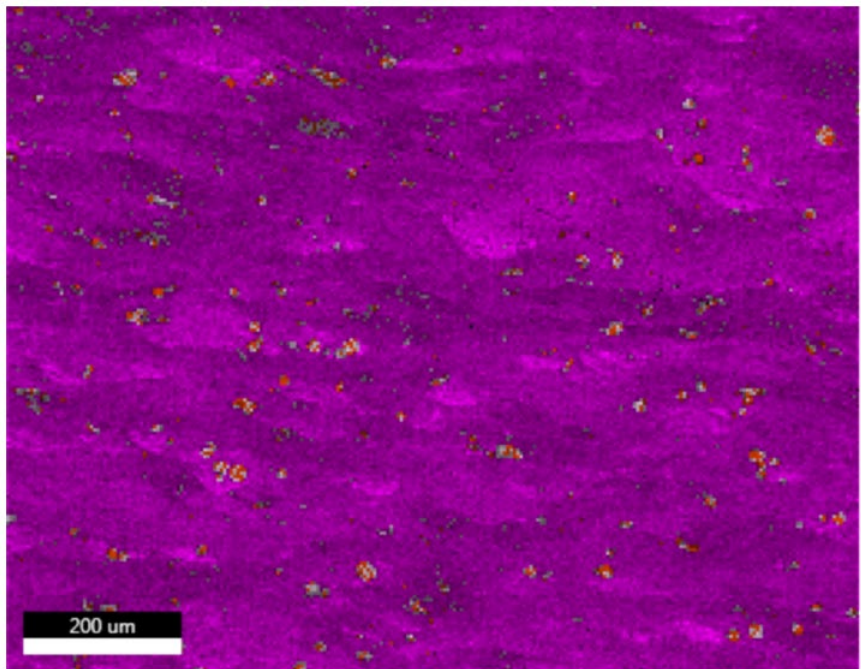
Table 4.8 Concentration of Mo, W, and Re at different printing speeds, heat treatment time, and heat treatment temperatures

Concentration at no Heat Treatment, 2000 C, and 2200 C						
Temperature (Celsius)	Heat Treatment (hours)	Speed (mm/s)	Mo (Weight%)	W (Weight%)	Re (Weight%)	
N/A	0	100	61.78	34.03	4.19	
N/A	0	400	71.01	25.77	3.22	
2000	12	100	74.09	22.58	3.33	
2000	12	400	70.55	28.62	0.83	
2200	6	100	67.87	29.27	2.86	
2200	6	400	65.53	34.47	0	

The complete homogeneity of some of these samples have not occurred since there are multiple phases instead of one uniform phase. The faster the printing speed, the less homogenous the alloy becomes, and the more phases appear. Figure 4.21 shows the progressive appearance of these phase as printing speed increases.



(a)



(b)

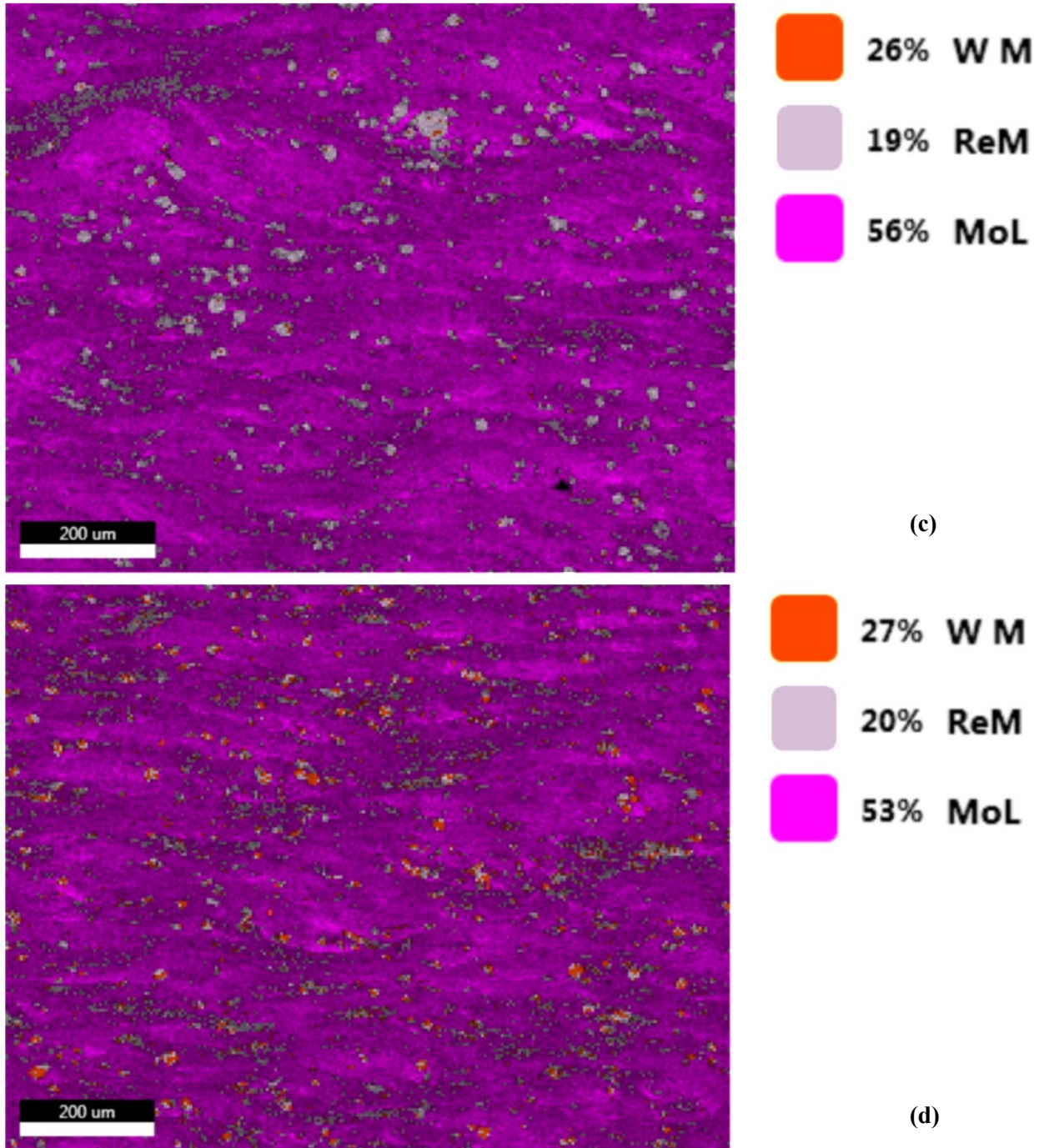


Figure 4.21 Phase diagram of 70Mo-25W-5Re printed at (a) 100 mm/s (b) 200 mm/s (c) 300 mm/s (d) 400 mm/s and heat treated for 4 hours

The concentration of the different phases remains consistent, but the presence of these phases increases as printing speed increases. For perfect homogenization to occur,

the colors would have to be consistent in these figures. Figure 4.21 only displayed the phase diagram of the samples heat treated at 1600 °C. Comparing the different heat treatment temperature shows an increase in homogenization. Figure 4.22 shows the different phases of tungsten at increasing heat treatment temperatures. At 1600 °C, the homogenization of tungsten appears to be like the sample that did not undergo heat treatment. However, homogenization appears to become more apparent at higher temperatures. At 2000 °C, homogenization of tungsten improves since there are less bright spots indicating phases. Further improvement in homogenization occurs at a higher temperature of 2200 °C. This indicates that even though 1600 °C had no significant effect in improving homogenization, there is potential for homogenization to improve at higher temperatures.

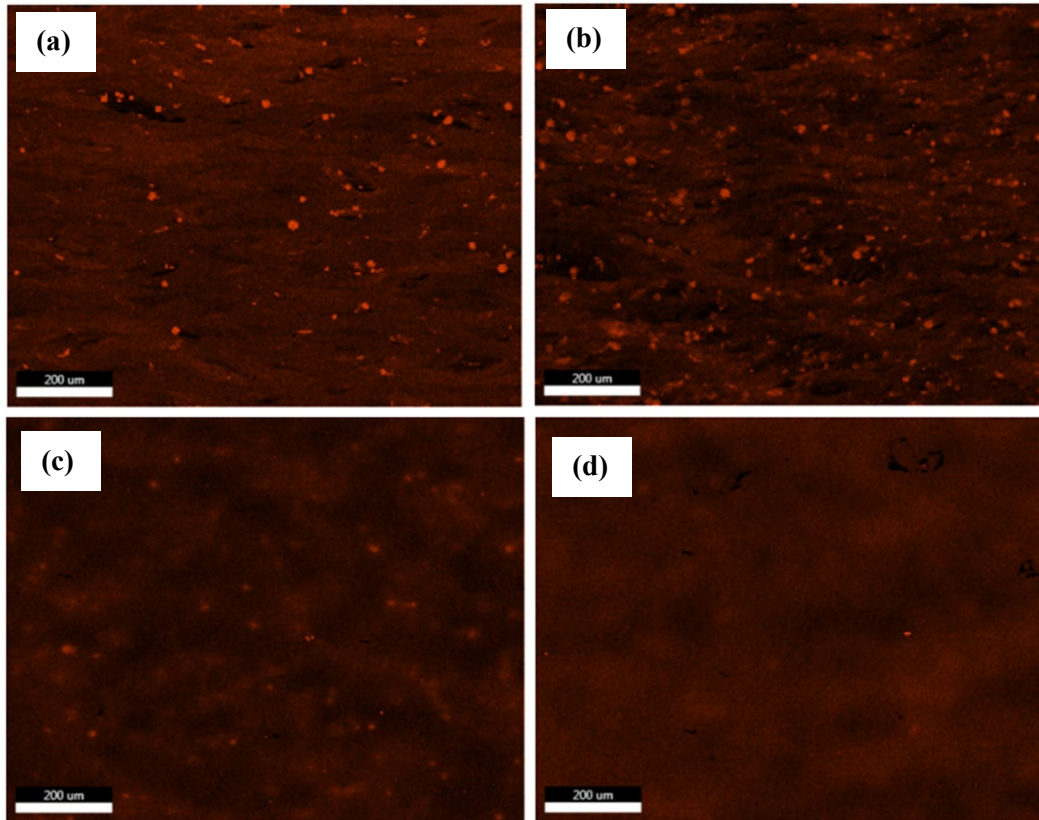


Figure 4.22 W phase diagram at (a) No Heat Treatment (b) 1600 °C (c) 2000 °C (d) 2200 °C printed at 400 mm/s

4.6 Summary

The bend test results provided valuable insight with how printing speed, shield gas composition, and heat treatment impacted strength and ductility. The Mo-30W alloys printed in argon-hydrogen gas came out to be stronger than alloys printed in argon. The analysis on the printing speed also proved that the slower printing speed provided samples with a higher strength and ductility. The average strength and percent strain of the 70Mo-25W-5Re also improves after undergoing heat treatment. The fracture surfaces observed through the SEM further proved how printing speed and shield gas composition affects the physical structures of the alloy. The observations through the SEM also

revealed that there are no significant microstructural changes developed from heat treatment at 1600 °C. The results of the hardness test provided evidence in the change of composition distribution through heat treatment. Comparing the hardness of the heat treated and non-heat-treated results indicate the material underwent a recovery process during heat treatment at 1600 °C. The porosity analysis is used to further prove the impacts of printing speed on porosity and the ineffectiveness of heat treatment reducing porosity. The EDS result showed that perfect homogeneity does not exist within the alloy. The faster printing speeds did show more phases than slower ones, but heat treatment did not significantly change the composition distribution and homogeneity of the alloy. Overall, the different parameter combinations prior to the bend test have proved that printing speeds, shield gas composition and heat treatment impact the different material properties of the alloy.

V. Conclusions and Recommendations

5.1 Shortcomings

The conclusions that are reached from this research are limited to the properties tested or analyzed. Due to the high cost of rhenium powders, the number of duplicate samples for each unique printing and heat-treating scenario is small. Having more trials can help improve an understanding of different trends that each heat-treatment style can provide. More sample replicates can help identify what trials are outliers and what trends are common.

Given the length of time to conduct this experiment, there is a limitation on how many differing heat-treated samples can be produced. Heat treatments at temperatures of 1600 °C, 2000 °C, and 2200 °C were chosen for this research, but having smaller increments in temperature may also help identify if there is a clear relationship between heat treatment temperature and strength and ductility.

5.2 Conclusions

This research has covered an analysis of the additively manufactured 70Mo-25W-5Re alloy. This alloy is observed and analyzed after being printed at different speeds and gaseous environments. Additionally, the effects of heat treating the additively manufactured alloy is observed and compared to other traditional tungsten alloys such as tungsten-molybdenum. Across the board, a slower printing speed that is printed with argon-hydrogen has proved to produce an alloy with a higher strength and percent strain value than that of an alloy printed with a faster speed with argon. The strength for the 70Mo-25W-5Re alloys also improved when they undergo heat treatment. Generally, the

length of time of heat treatment had no discernable impact to how much strength the alloy gains. Based on comparing the length of heat treatment time to stress, there has been no consistent trend on how much stronger or weaker an alloy gets the longer it is heat treated. Aside from the vertical samples printed at 100 mm/s, the ductility of the alloy has decreased with heat treatment. Like the case of the alloy's strength, there is no discernable relationship between heat treatment time and stress. Despite the effect heat treatment has done to the alloy's strength, results from other tests and evaluations show that the length of time that a sample is heat treated had no quantifiable impact in changing the alloy's hardness or porosity count. Recovery, indicated by hardness measurements, occurred very quickly at 1600 °C.

With the observations made with different heat treatment temperatures, the results are mixed. The ductility and strength improved significantly with the 45-degree sample printed at 100 mm/s and heat treated at 2000 °C. However, in other cases, the strength and ductility of some samples heat treated at 2000 °C are either worse or on par with samples heat treated at 1600 °C. The same goes with comparing samples heat treated at 1600 °C with samples heat treated at 2200 °C.

This research answered the questions laid out in Chapter 1. A mixture of elemental powders do not produce a completely homogeneous mixture through additive manufacturing, which affects the alloy's properties. For the 70Mo-25W-5Re alloys, heat treatment will also further increase the strength. The temperature the samples are heat treated show noticeable effects with the strength of the alloy. However, length of heat treatment time has no significance in changing the alloy's porosity, hardness, or homogeneity.

5.3 Future Recommendations

This work focused mostly on one combination of tungsten, molybdenum, and rhenium. There is an abundance of combinations that can be done with the study of these three metals in the alloy system. The only limit is figuring out combinations that avoid detrimental intermetallic phases. The properties of different alloy combinations can yield different results, and it is possible that there is an alloy combination that is more beneficial in terms of strength and density compared to 70Mo-25W-5Re. The heat treatment of the alloy in this research also focused on temperatures of 1600 °C, 2000 °C, and 2200 °C. It will be an interesting case study to see whether there is a trend between an alloy's strength and hardness with a higher or lower heat treatment temperature. Additional testing such as a high temperature bend test can provide a better understanding of how well this alloy can be used in a practical sense. Since tungsten alloys are used for its high heat resistance, it would be interesting to see how the 70Mo-25W-5Re alloy will fare and what strengths it maintains in an extremely hot environment. The EDS results only shows the metallic composition and phases of each alloy. However, this method is limited to detecting heavier elements due to the nature of its technique. Methods such as inert gas fusion can provide useful insights in future research. The process is useful in detecting lighter elements such as oxygen and hydrogen. Detecting these elements in the alloys can provide insight in determining how much of an influence these gasses have on strength, ductility, and homogeneity. There are many research paths when it comes to discovering a valuable alloy produced through additive manufacturing

Appendix A. Matlab Code

A.1 Stress Strain Data Processing for 1600 °C Heat Treated and Non-Heat-Treated Samples

```
1      %%%%%%%%%%%
2      %
3      % 70% Molybdenum 25% Tungsten 5% Rhenium manufactured by
selective laser melting
4      % 4-8-12-24hr Vacuumed Heated
5      % 100-200-300-400 Print Speed
6      % Vertical-45deg Orientation
7      % Bend Test Data
8      %
9      % Author: Maj Ryan Kemnitz
10     % Revised: Lt Jae Yu - 11 October 2021
11     %
12     %%%%%%%%%%%
13     %%
14     close all;clear all; clc
15
16     %% 4hr Heat Vertical
17     cd 'C:\70Mo20W5Re Heat Treated\4h\4h Vertical'
18     B = dir('**/*.txt');
19
20     for i = 1:length(B)
21         file = [B(i).folder,'\ ',B(i).name];
22         temp = importdata(file);
23
24         A{i} = -temp.data;
25
26         first_loc = find(A{i}(:,2)>2e-3,1);
27         A{i}(:,1) = A{i}(:,1)-A{i}(first_loc,1);
28
```

```

29     last_loc = find(A{i}(:,1)>0.5,1);
30     if isempty(last_loc) == true
31         last_loc = length(A{i}(:,1));
32     end
33
34     C{i} = A{i}(first_loc:last_loc-3,:);
35
36     [val(i,1),loc] = max(C{i}(:,2));
37     max_disp(i,1) = C{i}(loc,1);
38 end
39
40 speeds = [100;100;100;200;200;200;300;300;300;400;400;400];
41 unique_speeds = unique(speeds);
42 dims = importdata('MoWRe-4h-Measurements-v.xlsx');
43 widths = dims(:,1);
44 thicks = dims(:,2);
45
46 real_stress = 3*val*1000*14./(2*widths.*thicks.^2);
47 grind_newton=val;
48 real_strain = 6*max_disp.*thicks/14^2;
49
50 MOWRe4hrV_all = [speeds real_strain real_stress];
51 for i = 1:length(unique_speeds)
52     o = (i-1)*3+1;
53     p = i*3;
54     locs = find(speeds==unique_speeds(i));
55     average_stress(i) = mean(real_stress(locs));
56     average_strain(i,1) =100*mean(real_strain(locs));
57
58 end
59

```

```

60 EV = 200./(0.020*0.050*unique_speeds);
61
62
63 MOWRe4hrV = [unique_speeds EV average_stress' average_strain];
64 hold on
65 plot(real_strain*100,real_stress,'s','LineWidth',2); grid on
66
67
68 %% 4hr Heat 45 deg
69 clearvars -except MOWRe4hrV MOWRe4hrV_all
70
71 cd 'C:\70Mo20W5Re Heat Treated\4h\4h 45'
72 B = dir('**/*.txt');
73
74 for i = 1:length(B)
75     file = [B(i).folder,'\ ',B(i).name];
76     temp = importdata(file);
77
78     A{i} = -temp.data;
79
80     first_loc = find(A{i}(:,2)>2e-3,1);
81     A{i}(:,1) = A{i}(:,1)-A{i}(first_loc,1);
82
83     last_loc = find(A{i}(:,1)>0.5,1);
84     if isempty(last_loc) == true
85         last_loc = length(A{i}(:,1));
86     end
87
88     C{i} = A{i}(first_loc:last_loc-3,:);
89
90     [val(i,1),loc] = max(C{i}(:,2));

```

```

91     max_disp(i,1) = C{i}(loc,1);
92 end
93
94 speeds = [100;100;100;200;200;200;300;300;300;400;400];
95 unique_speeds = unique(speeds);
96
97 dims = importdata('MoWRe-4h-Measurements-45.xlsx');
98 widths = dims(:,1);
99 thicks = dims(:,2);
100
101 real_stress = 3*val*1000*14./(2*widths.*thicks.^2);
102 real_strain = 6*max_disp.*thicks/14^2;
103
104 MOWRe4hr45_all = [speeds real_strain real_stress];
105
106 for i = 1:length(unique_speeds)
107     o = (i-1)*3+1;
108     p = i*3;
109     locs = find(speeds==unique_speeds(i));
110     average_stress(i) = mean(real_stress(locs));
111     average_strain(i,1) =100*mean(real_strain(locs));
112
113 end
114
115 EV = 200./(0.020*0.050*unique_speeds);
116
117
118 MOWRe4hr45 = [unique_speeds EV average_stress' average_strain];
119 hold on
120 plot(real_strain*100,real_stress,'o','LineWidth',2)
121

```

```

122 %% 8hr Heat Vertical
123 clearvars -except MOWRe4hrV MOWRe4hrV_all MOWRe4hr45
MOWRe4hr45_all
124 cd 'C:\70Mo20W5Re Heat Treated\8h\8h Vertical'
125 B = dir('**/*.txt');
126
127 for i = 1:length(B)
128     file = [B(i).folder,'\',B(i).name];
129     temp = importdata(file);
130
131     A{i} = -temp.data;
132
133     first_loc = find(A{i}(:,2)>2e-3,1);
134     A{i}(:,1) = A{i}(:,1)-A{i}(first_loc,1);
135
136     last_loc = find(A{i}(:,1)>0.5,1);
137     if isempty(last_loc) == true
138         last_loc = length(A{i}(:,1));
139     end
140
141     C{i} = A{i}(first_loc:last_loc-3,:);
142
143     [val(i,1),loc] = max(C{i}(:,2));
144     max_disp(i,1) = C{i}(loc,1);
145 end
146
147 speeds = [100;100;100;200;200;200;300;300;300;400;400;400];
148 unique_speeds = unique(speeds);
149 dims = importdata('MoWRe-8h-Measurements-v.xlsx');
150 widths = dims(:,1);
151 thicks = dims(:,2);
152

```

```

153 real_stress = 3*val*1000*14./(2*widths.*thicks.^2);
154 grind_newton=val;
155 real_strain = 6*max_disp.*thicks/14^2;
156
157 MOWRe8hrV_all = [speeds real_strain real_stress];
158
159 for i = 1:length(unique_speeds)
160     o = (i-1)*3+1;
161     p = i*3;
162     locs = find(speeds==unique_speeds(i));
163     average_stress(i) = mean(real_stress(locs));
164     average_strain(i,1) =100*mean(real_strain(locs));
165
166 end
167
168 EV = 200./(0.020*0.050*unique_speeds);
169
170
171 MOWRe8hrV = [unique_speeds EV average_stress' average_strain];
172 hold on
173 plot(real_strain*100,real_stress,'s','LineWidth',2)
174
175
176 %% 8hr Heat 45 deg
177 clearvars -except MOWRe4hrV MOWRe4hrV_all MOWRe4hr45
MOWRe4hr45_all MOWRe8hrV MOWRe8hrV_all
178
179 cd 'C:\70Mo20W5Re Heat Treated\8h\8h 45'
180 B = dir('**/*.txt');
181
182 for i = 1:length(B)
183     file = [B(i).folder,'\',B(i).name];

```

```

184     temp = importdata(file);
185
186     A{i} = -temp.data;
187
188     first_loc = find(A{i}(:,2)>2e-3,1);
189     A{i}(:,1) = A{i}(:,1)-A{i}(first_loc,1);
190
191     last_loc = find(A{i}(:,1)>0.5,1);
192     if isempty(last_loc) == true
193         last_loc = length(A{i}(:,1));
194     end
195
196     C{i} = A{i}(first_loc:last_loc-3,:);
197
198     [val(i,1),loc] = max(C{i}(:,2));
199     max_disp(i,1) = C{i}(loc,1);
200 end
201
202 speeds = [100;100;100;200;200;200;300;300;300;400;400];
203 unique_speeds = unique(speeds);
204
205 dims = importdata('MoWRe-8h-Measurements-45.xlsx');
206 widths = dims(:,1);
207 thicks = dims(:,2);
208
209 real_stress = 3*val*1000*14./(2*widths.*thicks.^2);
210 real_strain = 6*max_disp.*thicks/14^2;
211
212 MOWRe8hr45_all = [speeds real_strain real_stress];
213
214 for i = 1:length(unique_speeds)

```

```

215     o = (i-1)*3+1;
216     p = i*3;
217     locs = find(speeds==unique_speeds(i));
218     average_stress(i) = mean(real_stress(locs));
219     average_strain(i,1) =100*mean(real_strain(locs));
220
221 end
222
223 EV = 200./(0.020*0.050*unique_speeds);
224
225
226 MOWRe8hr45 = [unique_speeds EV average_stress' average_strain];
227 hold on
228 plot(real_strain*100,real_stress,'o','LineWidth',2)
229
230 %% 12hr Heat Vertical
231 clearvars -except MOWRe4hrV MOWRe4hrV_all MOWRe4hr45
MOWRe4hr45_all ...
232     MOWRe8hrV MOWRe8hrV_all MOWRe8hr45 MOWRe8hr45_all
233 cd 'C:\70Mo20W5Re Heat Treated\12h\12h Vertical'
234 B = dir('**/*.txt');
235
236 figure
237 hold on
238 for i = 1:length(B);
239     file = [B(i).folder,'\',B(i).name];
240     temp = importdata(file);
241
242     A{i} = -temp.data;
243
244     first_loc = find(A{i}(:,2)>2e-3,1);
245     A{i}(:,1) = A{i}(:,1)-A{i}(first_loc,1);

```

```

246
247     last_loc = find(A{i}(:,1)>0.5,1);
248     if isempty(last_loc) == true
249         last_loc = length(A{i}(:,1));
250     end
251
252     C{i} = A{i}(first_loc:last_loc-3,:);
253
254     plot(C{i}(:,1),C{i}(:,2))
255     [val(i,1),loc] = max(C{i}(:,2));
256     max_disp(i,1) = C{i}(loc,1);
257 end
258
259 speeds = [100;100;100;200;200;200;300;300;300;400;400;400];
260 unique_speeds = unique(speeds);
261 dims = importdata('MoWRe-12h-Measurements-v.xlsx');
262 widths = dims(:,1);
263 thicks = dims(:,2);
264
265 real_stress = 3*val*1000*14./(2*widths.*thicks.^2);
266 grind_newton=val;
267 real_strain = 6*max_disp.*thicks/14^2;
268
269 MOWRe12hrV_all = [speeds real_strain real_stress];
270
271 for i = 1:length(unique_speeds)
272     o = (i-1)*3+1;
273     p = i*3;
274     locs = find(speeds==unique_speeds(i));
275     average_stress(i) = mean(real_stress(locs));
276     average_strain(i,1) =100*mean(real_strain(locs));

```

```

277
278 end
279
280 EV = 200./(0.020*0.050*unique_speeds);
281
282
283
legend('100 (1) ', '100 (2) ', '100 (3) ', '200 (1) ', '200 (2) ', '200 (3) ', '300 (1) ', '
300 (2) ', '300 (3) ', '400 (1) ', '400 (2) ', '400 (3) ')
284 hold off
285 figure
286 MOWRe12hrV = [unique_speeds EV average_stress' average_strain];
287 hold on
288 plot(real_strain*100,real_stress,'s','LineWidth',2)
289
290
291 %% 12hr Heat 45 deg
292 clearvars -except MOWRe4hrV MOWRe4hrV_all MOWRe4hr45
MOWRe4hr45_all ...
293 MOWRe8hrV MOWRe8hrV_all MOWRe8hr45 MOWRe8hr45_all MOWRe12hrV
MOWRe12hrV_all
294
295 cd 'C:\70Mo20W5Re Heat Treated\12h\12h 45'
296 B = dir('**/*.txt');
297
298 for i = 1:length(B)
299     file = [B(i).folder,'\',B(i).name];
300     temp = importdata(file);
301
302     A{i} = -temp.data;
303
304     first_loc = find(A{i}(:,2)>2e-3,1);
305     A{i}(:,1) = A{i}(:,1)-A{i}(first_loc,1);

```

```

306
307     last_loc = find(A{i}(:,1)>0.5,1);
308     if isempty(last_loc) == true
309         last_loc = length(A{i}(:,1));
310     end
311
312     C{i} = A{i}(first_loc:last_loc-3,:);
313
314     [val(i,1),loc] = max(C{i}(:,2));
315     max_disp(i,1) = C{i}(loc,1);
316 end
317
318 speeds = [100;100;100;200;200;200;300;300;300;400;400;400];
319 unique_speeds = unique(speeds);
320
321 dims = importdata('MoWRe-12h-Measurements-45.xlsx');
322 widths = dims(:,1);
323 thicks = dims(:,2);
324
325 real_stress = 3*val*1000*14./(2*widths.*thicks.^2);
326 real_strain = 6*max_disp.*thicks/14^2;
327
328 MOWRe12hr45_all = [speeds real_strain real_stress];
329
330 for i = 1:length(unique_speeds)
331     o = (i-1)*3+1;
332     p = i*3;
333     locs = find(speeds==unique_speeds(i));
334     average_stress(i) = mean(real_stress(locs));
335     average_strain(i,1) =100*mean(real_strain(locs));
336

```

```

337 end
338
339 EV = 200./(0.020*0.050*unique_speeds);
340
341
342 MOWRe12hr45 = [unique_speeds EV average_stress' average_strain];
343 hold on
344 plot(real_strain*100,real_stress,'o','LineWidth',2)
345
346 %% 24hr Heat Vertical
347 clearvars -except MOWRe4hrV MOWRe4hrV_all MOWRe4hr45
MOWRe4hr45_all ...
348     MOWRe8hrV MOWRe8hrV_all MOWRe8hr45 MOWRe8hr45_all ...
349     MOWRe12hrV MOWRe12hrV_all MOWRe12hr45 MOWRe12hr45_all
350 cd 'C:\70Mo20W5Re Heat Treated\24h\24h Vertical'
351 B = dir('**/*.txt');
352 figure
353 hold on
354 for i = 1:length(B);
355     file = [B(i).folder,'\ ',B(i).name];
356     temp = importdata(file);
357
358     A{i} = -temp.data;
359
360     first_loc = find(A{i}(:,2)>2e-3,1);
361     A{i}(:,1) = A{i}(:,1)-A{i}(first_loc,1);
362
363     last_loc = find(A{i}(:,1)>0.5,1);
364     if isempty(last_loc) == true
365         last_loc = length(A{i}(:,1));
366     end
367

```

```

368     C{i} = A{i}(first_loc:last_loc-3,:);
369     plot(C{i}(:,3),C{i}(:,1))
370     [val(i,1),loc] = max(C{i}(:,2));
371     max_disp(i,1) = C{i}(loc,1);
372 end
373
374 speeds = [100;100;100;200;200;200;300;300;300;400;400];
375 unique_speeds = unique(speeds);
376 dims = importdata('MoWRe-24h-Measurements-v.xlsx');
377 widths = dims(:,1);
378 thicks = dims(:,2);
379
380 real_stress = 3*val*1000*14./(2*widths.*thicks.^2);
381 grind_newton=val
382 real_strain = 6*max_disp.*thicks/14^2;
383
384 MOWRe24hrV_all = [speeds real_strain real_stress];
385
386 for i = 1:length(unique_speeds)
387     o = (i-1)*3+1;
388     p = i*3;
389     locs = find(speeds==unique_speeds(i));
390     average_stress(i) = mean(real_stress(locs));
391     average_strain(i,1) =100*mean(real_strain(locs));
392
393 end
394 legend('1','2','3','4','5','6','7','8','9','10')
395 EV = 200./(0.020*0.050*unique_speeds);
396 hold off
397 figure
398

```

```

399 MOWRe24hrV = [unique_speeds EV average_stress' average_strain];
400 hold on
401 plot(real_strain*100,real_stress,'s','LineWidth',2)
402
403
404 %% 24hr Heat 45 deg
405 clearvars -except MOWRe4hrV MOWRe4hrV_all MOWRe4hr45
MOWRe4hr45_all ...
406     MOWRe8hrV MOWRe8hrV_all MOWRe8hr45 MOWRe8hr45_all ...
407     MOWRe12hrV MOWRe12hrV_all MOWRe12hr45 MOWRe12hr45_all ...
408     MOWRe24hrV MOWRe24hrV_all
409
410 cd 'C:\70Mo20W5Re Heat Treated\24h\24h 45'
411 B = dir('**/*.txt');
412
413 for i = 1:length(B);
414     file = [B(i).folder,'\ ',B(i).name];
415     temp = importdata(file);
416
417     A{i} = -temp.data;
418
419     first_loc = find(A{i}(:,2)>2e-3,1);
420     A{i}(:,1) = A{i}(:,1)-A{i}(first_loc,1);
421
422     last_loc = find(A{i}(:,1)>0.5,1);
423     if isempty(last_loc) == true
424         last_loc = length(A{i}(:,1));
425     end
426
427     C{i} = A{i}(first_loc:last_loc-3,:);
428
429     [val(i,1),loc] = max(C{i}(:,2));

```

```

430     max_disp(i,1) = C{i}(loc,1);
431 end
432
433 speeds = [100;100;100;200;200;200;300;300;300;400;400;400];
434 unique_speeds = unique(speeds);
435
436 dims = importdata('MoWRe-24h-Measurements-45.xlsx');
437 widths = dims(:,1);
438 thicks = dims(:,2);
439
440 real_stress = 3*val*1000*14./(2*widths.*thicks.^2);
441 real_strain = 6*max_disp.*thicks/14^2;
442
443 MOWRe24hr45_all = [speeds real_strain real_stress];
444
445 for i = 1:length(unique_speeds)
446     o = (i-1)*3+1;
447     p = i*3;
448     locs = find(speeds==unique_speeds(i));
449     average_stress(i) = mean(real_stress(locs));
450     average_strain(i,1) =100*mean(real_strain(locs));
451
452 end
453
454 EV = 200./(0.020*0.050*unique_speeds);
455
456
457 MOWRe24hr45 = [unique_speeds EV average_stress' average_strain];
458 hold on
459 plot(real_strain*100,real_stress,'o','LineWidth',2)
460 %% 0hr Heat Vertical

```

```

461 clearvars -except MOWRe4hrV MOWRe4hrV_all MOWRe4hr45
MOWRe4hr45_all ...
462     MOWRe8hrV MOWRe8hrV_all MOWRe8hr45 MOWRe8hr45_all ...
463     MOWRe12hrV MOWRe12hrV_all MOWRe12hr45 MOWRe12hr45_all ...
464     MOWRe24hrV MOWRe24hrV_all MOWRe24hr45
465
466 cd 'C:\70Mo20W5Re Heat Treated\Non Heat Treated\Vertical'
467 B = dir('**/*.txt');
468
469 for i = 1:length(B);
470     file = [B(i).folder,'\ ',B(i).name];
471     temp = importdata(file);
472
473     A{i} = -temp.data;
474
475     first_loc = find(A{i}(:,2)>2e-3,1);
476     A{i}(:,1) = A{i}(:,1)-A{i}(first_loc,1);
477
478     last_loc = find(A{i}(:,1)>0.5,1);
479     if isempty(last_loc) == true
480         last_loc = length(A{i}(:,1));
481     end
482
483     C{i} = A{i}(first_loc:last_loc-3,:);
484
485     [val(i,1),loc] = max(C{i}(:,2));
486     max_disp(i,1) = C{i}(loc,1);
487 end
488
489 speeds =
[100;100;100;200;200;225;225;225;400;400;600;600;600;800;800];
490 unique_speeds = unique(speeds);

```

```

491
492 dims = importdata('MoMeasurement_V.xlsx');
493 widths = dims(:,1);
494 thicks = dims(:,2);
495
496 real_stress = 3*val*1000*14./(2*widths.*thicks.^2);
497 real_strain = 6*max_disp.*thicks/14^2;
498
499 MOWRe0hrV_all = [speeds real_strain real_stress];
500
501 for i = 1:length(unique_speeds)
502     o = (i-1)*3+1;
503     p = i*3;
504     locs = find(speeds==unique_speeds(i));
505     average_stress(i) = mean(real_stress(locs));
506     average_strain(i,1) =100*mean(real_strain(locs));
507
508 end
509
510 EV = 200./(0.020*0.050*unique_speeds);
511
512
513 MOWRe0hrV = [unique_speeds EV average_stress' average_strain];
514 hold on
515 plot(real_strain*100,real_stress,'o','LineWidth',2)
516
517 %% 0hr Heat 45
518 clearvars -except MOWRe4hrV MOWRe4hrV_all MOWRe4hr45
MOWRe4hr45_all ...
519     MOWRe8hrV MOWRe8hrV_all MOWRe8hr45 MOWRe8hr45_all ...
520     MOWRe12hrV MOWRe12hrV_all MOWRe12hr45 MOWRe12hr45_all ...
521     MOWRe24hrV MOWRe24hrV_all MOWRe24hr45 MOWRe0hrV MOWRe0hrV_all

```

```

522
523 cd 'C:\70Mo20W5Re Heat Treated\Non Heat Treated\45'
524 B = dir('**/*.txt');
525
526 for i = 1:length(B);
527     file = [B(i).folder,'\ ',B(i).name];
528     temp = importdata(file);
529
530     A{i} = -temp.data;
531
532     first_loc = find(A{i}(:,2)>2e-3,1);
533     A{i}(:,1) = A{i}(:,1)-A{i}(first_loc,1);
534
535     last_loc = find(A{i}(:,1)>0.5,1);
536     if isempty(last_loc) == true
537         last_loc = length(A{i}(:,1));
538     end
539
540     C{i} = A{i}(first_loc:last_loc-3,:);
541
542     [val(i,1),loc] = max(C{i}(:,2));
543     max_disp(i,1) = C{i}(loc,1);
544 end
545
546 speeds =
[100;100;100;200;200;200;400;400;400;600;600;600;800;800;800];
547 unique_speeds = unique(speeds);
548
549 dims = importdata('MoMeasurement_45.xlsx');
550 widths = dims(:,1);
551 thicks = dims(:,2);
552

```

```

553 real_stress = 3*val*1000*14./(2*widths.*thicks.^2);
554 real_strain = 6*max_disp.*thicks/14^2;
555
556 MOWRe0hr45_all = [speeds real_strain real_stress];
557
558 for i = 1:length(unique_speeds)
559     o = (i-1)*3+1;
560     p = i*3;
561     locs = find(speeds==unique_speeds(i));
562     average_stress(i) = mean(real_stress(locs));
563     average_strain(i,1) =100*mean(real_strain(locs));
564
565 end
566
567 EV = 200./(0.020*0.050*unique_speeds);
568
569
570 MOWRe0hr45 = [unique_speeds EV average_stress' average_strain];
571 hold on
572 plot(real_strain*100,real_stress,'o','LineWidth',2)
573
574 %%
575 title('70% Molybdenum 25% Tungsten 5% Rhenium Strain vs Stress')
576 xlabel('Strain (dimensionless)')
577 ylabel('Stress (Newton/milimeter^2)')
578 legend('MoWRe 4hr V','MoWRe 4hr 45','MoWRe 8hr V','MoWRe 8hr
45',...
579         'MoWRe 12hr V','MoWRe 12hr 45','MoWRe 24hr V','MoWRe 24hr
45',...
580         'MoWRe 0hr V','MoWRe 0hr 45')
581 %%
582 % missing 4hr 45 400 data

```

```

583 % missing 8hr 45 400 data
584 % missing 24hr v 400 data
585
586 %%
587 figure
588 plot(MOWRe4hrV(:,4),MOWRe4hrV(:,3),'s','LineWidth',2)
589 hold on
590 plot(MOWRe4hr45(:,4),MOWRe4hr45(:,3),'o','LineWidth',2)
591 plot(MOWRe8hrV(:,4),MOWRe8hrV(:,3),'s','LineWidth',2)
592 plot(MOWRe8hr45(:,4),MOWRe8hr45(:,3),'o','LineWidth',2)
593 plot(MOWRe12hrV(:,4),MOWRe12hrV(:,3),'s','LineWidth',2)
594 plot(MOWRe12hr45(:,4),MOWRe12hr45(:,3),'o','LineWidth',2)
595 plot(MOWRe24hrV(:,4),MOWRe24hrV(:,3),'s','LineWidth',2)
596 plot(MOWRe24hr45(:,4),MOWRe24hr45(:,3),'o','LineWidth',2)
597 plot(MOWRe0hrV(:,4),MOWRe0hrV(:,3),'x','LineWidth',2)
598 plot(MOWRe0hr45(:,4),MOWRe0hr45(:,3),'+','LineWidth',2)
599 grid on
600 title('70% Molybdenum 25% Tungsten 5% Rhenium Average Strain vs
Stress')
601 xlabel('Strain (dimensionless)')
602 ylabel('Stress (Newton/milimeter^2)')
603
604 legend('MoWRe 4hr V','MoWRe 4hr 45','MoWRe 8hr V','MoWRe 8hr
45',...
605         'MoWRe 12hr V','MoWRe 12hr 45','MoWRe 24hr V','MoWRe 24hr
45',...
606         'MoWRe 0hr V','MoWRe 0hr 45')
607 axis([0.4 1.9 0 700])

```

A.2 Stress Strain Processing for 2000 °C and 2200 °C Heat Treated Samples

```

1 %%%%%%%%%%%%%%%%%%%%%%%%%%%%%%%%%%%%%%%%%
2 %

```

```

3      % 70% Molybdenum 25% Tungsten 5% Rhenium manufactured by
selective laser melting
4      % Heat Treated in 2000C and 2200C
5      % 100-400 Print Speed
6      % Vertical-45deg Orientation
7      % Bend Test Data
8      %
9      % Author: Maj Ryan Kemnitz
10     % Revised: Lt Jae Yu - 11 October 2021
11     %
12     %%%%%%%%%%%
13     %%
14     close all;clear all; clc
15
16     %% 2000C 12hr Heat Vertical
17     cd 'C:\70Mo20W5Re Heat Treated\Other HT RT\2000C_12hr_v'
18     B = dir('**/*.txt');
19
20     for i = 1:length(B)
21         file = [B(i).folder,'\ ',B(i).name];
22         temp = importdata(file);
23
24         A{i} = -temp.data;
25
26         first_loc = find(A{i}(:,2)>2e-3,1);
27         A{i}(:,1) = A{i}(:,1)-A{i}(first_loc,1);
28
29         last_loc = find(A{i}(:,1)>0.5,1);
30         if isempty(last_loc) == true
31             last_loc = length(A{i}(:,1));
32         end
33

```

```

34     C{i} = A{i}(first_loc:last_loc-3,:);
35
36     [val(i,1),loc] = max(C{i}(:,2));
37     max_disp(i,1) = C{i}(loc,1);
38 end
39
40 speeds = [100;100;100;400;400;400];
41 unique_speeds = unique(speeds);
42 dims = importdata('MoWRe-2000C-Measurements-v.xlsx');
43 widths = dims(:,1);
44 thicks = dims(:,2);
45
46 real_stress = 3*val*1000*14./(2*widths.*thicks.^2);
47 grind_newton=val;
48 real_strain = 6*max_disp.*thicks/14^2;
49
50 MOWRe2000C_V_all = [speeds real_strain real_stress];
51 for i = 1:length(unique_speeds)
52     o = (i-1)*3+1;
53     p = i*3;
54     locs = find(speeds==unique_speeds(i));
55     average_stress(i) = mean(real_stress(locs));
56     average_strain(i,1) =100*mean(real_strain(locs));
57
58 end
59
60 EV = 200./(0.020*0.050*unique_speeds);
61
62
63 MOWRe2000C_V = [unique_speeds EV average_stress' average_strain];
64 hold on

```

```

65 plot(real_strain*100,real_stress,'s','LineWidth',2); grid on
66
67
68 %% 2000C 12hr Heat 45 deg
69 clearvars -except MOWRe2000C_V MOWRe2000C_V_all
70
71 cd 'C:\70Mo20W5Re Heat Treated\Other HT RT\2000C_12h_45'
72 B = dir('**/*.txt');
73
74 for i = 1:length(B)
75     file = [B(i).folder,'\',B(i).name];
76     temp = importdata(file);
77
78     A{i} = -temp.data;
79
80     first_loc = find(A{i}(:,2)>2e-3,1);
81     A{i}(:,1) = A{i}(:,1)-A{i}(first_loc,1);
82
83     last_loc = find(A{i}(:,1)>0.5,1);
84     if isempty(last_loc) == true
85         last_loc = length(A{i}(:,1));
86     end
87
88     C{i} = A{i}(first_loc:last_loc-3,:);
89
90     [val(i,1),loc] = max(C{i}(:,2));
91     max_disp(i,1) = C{i}(loc,1);
92 end
93
94 speeds = [100;100;100;400;400;400];
95 unique_speeds = unique(speeds);

```

```

96
97     dims = importdata('MoWRe-2000C-Measurements-45.xlsx');
98     widths = dims(:,1);
99     thicks = dims(:,2);
100
101     real_stress = 3*val*1000*14./(2*widths.*thicks.^2);
102     real_strain = 6*max_disp.*thicks/14^2;
103
104     MOWRe2000C_45_all = [speeds real_strain real_stress];
105
106     for i = 1:length(unique_speeds)
107         o = (i-1)*3+1;
108         p = i*3;
109         locs = find(speeds==unique_speeds(i));
110         average_stress(i) = mean(real_stress(locs));
111         average_strain(i,1) =100*mean(real_strain(locs));
112
113     end
114
115     EV = 200./(0.020*0.050*unique_speeds);
116
117
118     MOWRe2000C_45 = [unique_speeds EV average_stress'
119     average_strain];
120
121     hold on
122     plot(real_strain*100,real_stress,'o','LineWidth',2)
123
124     %% 2200C 6hr Heat Vertical
125     clearvars -except MOWRe2000C_V MOWRe2000C_V_all MOWRe2000C_45
126     MOWRe2000C_45_all
127     cd 'C:\70Mo20W5Re Heat Treated\Other HT RT\2200C_6h_v'
128     B = dir('**/*.txt');

```

```

126
127 for i = 1:length(B)
128     file = [B(i).folder,'\ ',B(i).name];
129     temp = importdata(file);
130
131     A{i} = -temp.data;
132
133     first_loc = find(A{i}(:,2)>2e-3,1);
134     A{i}(:,1) = A{i}(:,1)-A{i}(first_loc,1);
135
136     last_loc = find(A{i}(:,1)>0.5,1);
137     if isempty(last_loc) == true
138         last_loc = length(A{i}(:,1));
139     end
140
141     C{i} = A{i}(first_loc:last_loc-3,:);
142
143     [val(i,1),loc] = max(C{i}(:,2));
144     max_disp(i,1) = C{i}(loc,1);
145 end
146
147 speeds = [100;100;100;400;400;400];
148 unique_speeds = unique(speeds);
149 dims = importdata('MoWRe-2200C-Measurements-v.xlsx');
150 widths = dims(:,1);
151 thicks = dims(:,2);
152
153 real_stress = 3*val*1000*14./(2*widths.*thicks.^2);
154 grind_newton=val;
155 real_strain = 6*max_disp.*thicks/14^2;
156

```

```

157 MOWRe2200C_V_all = [speeds real_strain real_stress];
158
159 for i = 1:length(unique_speeds)
160     o = (i-1)*3+1;
161     p = i*3;
162     locs = find(speeds==unique_speeds(i));
163     average_stress(i) = mean(real_stress(locs));
164     average_strain(i,1) =100*mean(real_strain(locs));
165
166 end
167
168 EV = 200./(0.020*0.050*unique_speeds);
169
170
171 MOWRe2200C_V = [unique_speeds EV average_stress' average_strain];
172 hold on
173 plot(real_strain*100,real_stress,'s','LineWidth',2)
174
175 %%
176 title('70% Molybdenum 25% Tungsten 5% Rhenium Strain vs Stress')
177 xlabel('Strain (dimensionless)')
178 ylabel('Stress (Newton/milimeter^2)')
179 legend('MoWRe 2000C 12h V','MoWRe 2000C 12h 45','MoWRe 2200C 6h
V')
180 %%
181 figure
182 plot(MOWRe2000C_V(:,4),MOWRe2000C_V(:,3),'s','LineWidth',2)
183 hold on
184 plot(MOWRe2000C_45(:,4),MOWRe2000C_45(:,3),'o','LineWidth',2)
185 plot(MOWRe2200C_V(:,4),MOWRe2200C_V(:,3),'s','LineWidth',2)
186 grid on
187 title('70% Mo 25% W 5% Re Average Strain vs Stress')

```

```

188 xlabel('Strain (dimensionless)')
189 ylabel('Stress (Newton/milimeter^2)')
190
191 legend('MoWRe 2000C 12h V','MoWRe 2000C 12h 45','MoWRe 2200C 6h
V')
192 axis([0.4 2.5 0 700])
193
194 %% Export Data to Excel
195 cd 'C:\70Mo20W5Re Heat Treated\Stress Strain Value\All Stress
Strain\Vertical'
196 xlswrite('MoWRe 2000C 12hr V all.xlsx',MOWRe2000C_V_all)
197 xlswrite('MoWRe 2200C 6hr V all.xlsx',MOWRe2200C_V_all)
198
199
200 cd 'C:\70Mo20W5Re Heat Treated\Stress Strain Value\All Stress
Strain\45'
201 xlswrite('MoWRe 2000C 12hr 45 all.xlsx',MOWRe2000C_45_all)
202

```

A.3 Heat Treatment Temperature vs Stress and Strain Code

```

1 clc;clear all;close all
2 cd 'C:\70Mo20W5Re Heat Treated\Stress Strain Value\All Stress
Strain\Vertical'
3 MoWRe1600_100_v=importdata('100mms at 1600C v.xlsx');
4 MoWRe1600_200_v=importdata('200mms at 1600C v.xlsx');
5 MoWRe1600_300_v=importdata('300mms at 1600C v.xlsx');
6 MoWRe1600_400_v=importdata('400mms at 1600C v.xlsx');
7
8 MoWRe2000data=importdata('MoWRe 2000C 12hr V all.xlsx'); %12 hour
HT only
9 MoWRe2000_100_v=MoWRe2000data(1:3,2:3);
10 MoWRe2000_400_v=MoWRe2000data(4:6,2:3);
11

```

```

12     MoWRe2200data=importdata('MoWRe 2200C 6hr V all.xlsx'); %6 hour
HT only
13     MoWRe2200_100_v=MoWRe2200data(1:3,2:3);
14     MoWRe2200_400_v=MoWRe2200data(4:6,2:3);
15
16     cd 'C:\70Mo20W5Re Heat Treated\Stress Strain Value\All Stress
Strain\45'
17     MoWRe1600_100_45=importdata('100mms at 1600C 45.xlsx');
18     MoWRe1600_200_45=importdata('200mms at 1600C 45.xlsx');
19     MoWRe1600_300_45=importdata('300mms at 1600C 45.xlsx');
20     MoWRe1600_400_45=importdata('400mms at 1600C 45.xlsx');
21
22     MoWRe2000data=importdata('MoWRe 2000C 12hr 45 all.xlsx'); %12
hour HT only
23     MoWRe2000_100_45=MoWRe2000data(1:3,2:3);
24     MoWRe2000_400_45=MoWRe2000data(4:6,2:3);
25
26     %% Stress plots
27
28     % Vertical Stress for 1600C
29     figure()
30     subplot(2,2,1)
31     plot(MoWRe1600_100_v(:,1),MoWRe1600_100_v(:,3),'o','LineWidth',2)
32     title('100 mm/s')
33     grid on
34     xlabel('Heat Treatment Time (hours)')
35     ylabel('Stress (N/mm^2)')
36     axis([0 24 0 700])
37
38     subplot(2,2,2)
39     plot(MoWRe1600_200_v(:,1),MoWRe1600_200_v(:,3),'o','LineWidth',2)
40     title('200 mm/s')

```

```

41  grid on
42  xlabel('Heat Treatment Time (hours)')
43  ylabel('Stress (N/mm^2)')
44  axis([0 24 0 700])
45
46  subplot(2,2,3)
47  plot(MoWRe1600_300_v(:,1),MoWRe1600_300_v(:,3),'o','LineWidth',2)
48  title('300 mm/s')
49  grid on
50  xlabel('Heat Treatment Time (hours)')
51  ylabel('Stress (N/mm^2)')
52  axis([0 24 0 700])
53
54  subplot(2,2,4)
55  plot(MoWRe1600_400_v(:,1),MoWRe1600_400_v(:,3),'o','LineWidth',2)
56  title('400 mm/ss')
57  grid on
58  xlabel('Heat Treatment Time (hours)')
59  ylabel('Stress (N/mm^2)')
60  axis([0 24 0 700])
61
62  sgtitle('Stress vs Heat Treatment Time per Vertical Print Speed')
63
64  %45 degree Stress at 1600C
65  figure()
66  subplot(2,2,1)
67
68  plot(MoWRe1600_100_45(:,1),MoWRe1600_100_45(:,3),'o','LineWidth',2)
69  title('100 mm/s')
70  grid on
71  xlabel('Heat Treatment Time (hours)')
72  ylabel('Stress (N/mm^2)')

```

```

72     axis([0 24 0 700])
73
74     subplot(2,2,2)
75
76     plot(MoWRe1600_200_45(:,1),MoWRe1600_200_45(:,3),'o','LineWidth',2)
77
78     title('200 mm/s')
79     grid on
80     xlabel('Heat Treatment Time (hours)')
81     ylabel('Stress (N/mm^2)')
82     axis([0 24 0 700])
83
84     subplot(2,2,3)
85
86     plot(MoWRe1600_300_45(:,1),MoWRe1600_300_45(:,3),'o','LineWidth',2)
87
88     title('300 mm/s')
89     grid on
90     xlabel('Heat Treatment Time (hours)')
91     ylabel('Stress (N/mm^2)')
92     axis([0 24 0 700])
93
94     subplot(2,2,4)
95
96     plot(MoWRe1600_400_45(:,1),MoWRe1600_400_45(:,3),'o','LineWidth',2)
97
98     title('400 mm/ss')
99     grid on
100    xlabel('Heat Treatment Time (hours)')
101    ylabel('Stress (N/mm^2)')
102    axis([0 24 0 700])
103
104    sgtitle('Stress vs Heat Treatment Time per 45 Print Speed')
105
106
107
108
109
110

```

```

101 %% Strain Plots
102
103 figure()
104 subplot(2,2,1)
105
106 plot(MoWRel600_100_v(:,1),MoWRel600_100_v(:,2)*100,'o','LineWidth',2)
107
108 title('100 mm/s')
109 grid on
110 xlabel('Heat Treatment Time (hours)')
111 ylabel('Strain')
112 axis([0 24 0.4 1.9])
113
114 subplot(2,2,2)
115
116 plot(MoWRel600_200_v(:,1),MoWRel600_200_v(:,2)*100,'o','LineWidth',2)
117
118 title('200 mm/s')
119 grid on
120 xlabel('Heat Treatment Time (hours)')
121 ylabel('Strain')
122 axis([0 24 0.4 1.9])
123
124 subplot(2,2,3)
125
126 plot(MoWRel600_300_v(:,1),MoWRel600_300_v(:,2)*100,'o','LineWidth',2)
127
128 title('300 mm/s')
129 grid on
130 xlabel('Heat Treatment Time (hours)')
131 ylabel('Strain')
132 axis([0 24 0.4 1.9])
133
134 subplot(2,2,4)
135
136 plot(MoWRel600_400_v(:,1),MoWRel600_400_v(:,2)*100,'o','LineWidth',2)

```

```

130 title('400 mm/ss')
131 grid on
132 xlabel('Heat Treatment Time (hours)')
133 ylabel('Strain')
134 axis([0 24 0.4 1.9])
135
136 sgtitle('Strain vs Heat Treatment Time per Vertical Print Speed')
137
138 %45 degree strain at 1600C
139 figure()
140 subplot(2,2,1)
141
142 plot(MoWRe1600_100_45(:,1),MoWRe1600_100_45(:,2)*100,'o','LineWidth',2)
143 title('100 mm/s')
144 grid on
145 xlabel('Heat Treatment Time (hours)')
146 ylabel('Strain')
147 axis([0 24 0.4 1.9])
148
149 subplot(2,2,2)
150
151 plot(MoWRe1600_200_45(:,1),MoWRe1600_200_45(:,2)*100,'o','LineWidth',2)
152 title('200 mm/s')
153 grid on
154 xlabel('Heat Treatment Time (hours)')
155 ylabel('Strain')
156 axis([0 24 0.4 1.9])
157
158 subplot(2,2,3)
159
160 plot(MoWRe1600_300_45(:,1),MoWRe1600_300_45(:,2)*100,'o','LineWidth',2)
161 title('300 mm/s')

```

```

159  grid on
160  xlabel('Heat Treatment Time (hours)')
161  ylabel('Strain')
162  axis([0 24 0.4 1.9])
163
164  subplot(2,2,4)
165
166  plot(MoWRe1600_400_45(:,1),MoWRe1600_400_45(:,2)*100,'o','LineWidth',2)
167  title('400 mm/ss')
168  grid on
169  xlabel('Heat Treatment Time (hours)')
170  ylabel('Strain')
171  axis([0 24 0.4 1.9])
172
173  sgtitle('Strain vs Heat Treatment Time per 45 Print Speed')
174  %% 2000C and 2200C
175  figure()
176  subplot(2,1,1)
177
178  plot(MoWRe1600_100_v(10:12,2)*100,MoWRe1600_100_v(10:12,3),'o','LineWid
179  th',2)
180  hold on
181
182  plot(MoWRe2000_100_v(:,1)*100,MoWRe2000_100_v(:,2),'s','LineWidth',2)
183  title('100 mm/s')
184  grid on
185  axis([0.4 2.5 0 700])
186  xlabel('Strain (dimensionless)')
187  ylabel('Stress (Newton/milimeter^2)')
188  legend('1600 C','2000 C')
189
190  subplot(2,1,2)

```

```

187
plot(MoWRe1600_400_v(10:12,2)*100,MoWRe1600_400_v(10:12,3),'o','LineWid
th',2)

188 hold on

189
plot(MoWRe2000_400_v(:,1)*100,MoWRe2000_400_v(:,2),'s','LineWidth',2)
190 title('400 mm/s')
191 grid on
192 axis([0.4 2.5 0 700])
193 xlabel('Strain (dimensionless)')
194 ylabel('Stress (Newton/milimeter^2)')
195 legend('1600 C','2000 C')
196
197 sgtitle('Strain vs Stress Vertical 12h')
198
199 %45 degree
200 figure()
201 subplot(2,1,1)
202
plot(MoWRe1600_100_45(10:12,2)*100,MoWRe1600_100_45(10:12,3),'o','LineW
idth',2)

203 hold on

204
plot(MoWRe2000_100_45(:,1)*100,MoWRe2000_100_45(:,2),'s','LineWidth',2)
205 title('100 mm/s')
206 grid on
207 axis([0.4 3.5 0 700])
208 xlabel('Strain (dimensionless)')
209 ylabel('Stress (Newton/milimeter^2)')
210 legend('1600 C','2000 C')
211
212 subplot(2,1,2)

```

```

213
plot(MoWRe1600_400_45(10:12,2)*100,MoWRe1600_400_45(10:12,3),'o','LineW
idth',2)

214  hold on

215
plot(MoWRe2000_400_45(:,1)*100,MoWRe2000_400_45(:,2),'s','LineWidth',2)
216  title('400 mm/s')
217  grid on
218  axis([0.4 2.4 0 700])
219  xlabel('Strain (dimensionless)')
220  ylabel('Stress (Newton/milimeter^2)')
221  legend('1600 C','2000 C')
222
223  sgtitle('Strain vs Stress 45 degree 12h')
224
225  %2200C
226
227  figure()
228  subplot(2,1,1)
229
plot(MoWRe1600_100_v(4:6,2)*100,MoWRe1600_100_v(4:6,3),'o','LineWidth',
2)

230  hold on

231
plot(MoWRe1600_100_v(7:9,2)*100,MoWRe1600_100_v(7:9,3),'o','LineWidth',
2)

232
plot(MoWRe2200_100_v(:,1)*100,MoWRe2200_100_v(:,2),'s','LineWidth',2)
233  title('100 mm/s')
234  grid on
235  axis([0.4 2.5 0 700])
236  xlabel('Strain (dimensionless)')
237  ylabel('Stress (Newton/milimeter^2)')
238  legend('1600 C 4hr','1600 C 8 hr','2200 C 6 hr')

```

```
239
240 subplot(2,1,2)
241
242 plot(MoWRe1600_400_v(3:5,2)*100,MoWRe1600_400_v(3:5,3),'o','LineWidth',
2)
242 hold on
243
244 plot(MoWRe1600_400_v(6:8,2)*100,MoWRe1600_400_v(6:8,3),'o','LineWidth',
2)
244
245 plot(MoWRe2200_400_v(:,1)*100,MoWRe2200_400_v(:,2),'s','LineWidth',2)
245 title('400 mm/s')
246 grid on
247 axis([0.2 2.4 0 700])
248 xlabel('Strain (dimensionless)')
249 ylabel('Stress (Newton/milimeter^2)')
250 legend('1600 C 4hr','1600 C 8 hr','2200 C 6 hr')
251 sgtitle('Strain vs Stress Vertical')
```

Bibliography

- [1] A. Bradford, "Facts about Tungsten," 2016. [Online]. Available: <https://www.livescience.com/38997-facts-about-tungsten.html>.
- [2] O. D. Neikov and N. A. Yefimov, "Nanopowders," in *Handbook of Non-Ferrous Metal Powders*, Elsevier, 2019, pp. 271-311.
- [3] "Molybdenum - Element information, properties and uses | Periodic Table," [Online]. Available: <https://www.rsc.org/periodic-table/element/42/molybdenum>.
- [4] J. E., Rhenium : Properties, Uses, and Occurrence, Nova Science Publishers, 2017.
- [5] T. Wohlers and T. Gornet, "History of additive manufacturing," *Wohlers report*, vol. 24, no. 2014, p. 118, 2014.
- [6] A. Mokrane, M. Boutaous and S. Xin, "Process of selective laser sintering of polymer powders: Modeling, simulation, and validation," *Comptes Rendus Mécanique*, vol. 346, no. 11, pp. 1087-1103, 2018.
- [7] C. G. Vayenas, R. E. W. and M. E. Gamboa-Aldeco, "Induced Codeposition of Alloys of Tungsten, Molybdenum and Rhenium with Transition Metals," in *Modern Aspects of Electrochemistry*, Springer Science & Business Media, 2008, pp. 191-301.
- [8] J. Braun, L. Kaserer, J. Stajkovic, K.-H. Leitz, B. Tabernig, P. Singer, I. Letofsky-Papst, H. Kestler and G. Leichtfried, "Fully dense and crack free molybdenum manufactured by Selective Laser Melting through alloying with carbon," *International Journal of Refractory Metals & Hard Materials*, pp. 1-8, 2019.

- [9] S. Johnson and D. Burns, "Chapter: Nuclear Thermal Propulsion Reactor Materials," IntechOpen, 10 March 2020. [Online]. Available: <https://www.intechopen.com/chapters/71396>.
- [10] L. Shen, X. Li, D. Lindberg and P. Taskinen, "Tungsten extractive metallurgy: A review of processes and their challenges for sustainability," *Minerals Engineering*, vol. 142, p. 105934, 2019.
- [11] M. Xiao, F. Li, H. Xie and Y. Wang, "Characterization of strengthening mechanism and hot deformation behavior of powder metallurgy molybdenum," *Materials & Design*, vol. 34, pp. 112-119, 2012.
- [12] E. Lassner and W.-D. Schubert, Tungsten: properties, chemistry, technology of the element, alloys, and chemical compounds, New York: Kluwer Academic/Plenum Publishers, 1999.
- [13] Z.-Y. Zeng, C.-E. Hu, L.-C. Cai, X.-R. Chen and F.-Q. Jing, "Lattice Dynamics and Thermodynamics of Molybdenum from First-Principles Calculations," *The Journal of Physical Chemistry*, vol. 114, no. 1, pp. 298-310, 2010.
- [14] "1.6: Structure and bonding - crystal structure," Libretexts, [Online]. Available: [https://chem.libretexts.org/Bookshelves/Inorganic_Chemistry/Chemistry_of_the_Main_Group_Elements_\(Barron\)/01%3A_General_Concepts_and_Trends/1.06%3A_Structure_and_Bonding_-_Crystal_Structure](https://chem.libretexts.org/Bookshelves/Inorganic_Chemistry/Chemistry_of_the_Main_Group_Elements_(Barron)/01%3A_General_Concepts_and_Trends/1.06%3A_Structure_and_Bonding_-_Crystal_Structure).
- [15] S. V. Nagender and P. R. Rao, Phase Diagrams of Binary Tungsten Alloys, Calcutta: Indian Institute of Metals, 1991.

- [16] E. Pink and e. al, "Refractory Metals and Their Alloys," in *Materials Science and Technology*, Weinheim, 1996, pp. 591-638.
- [17] N. Eliaz and G. Eliezer, "Induced codeposition of alloys of tungsten, molybdenum and rhenium with transition metals," in *Modern aspects of electrochemistry*, New York, Springer, 2008, pp. 191-301.
- [18] E. Lassner, W. D. Schubert, E. Ludertiz and H. U. Wolf, "Tungsten. Tungsten Alloys, and Tungsten Compounds,," *Ullmann's Encyclopedia of Industrial Chemistry*, vol. A27, pp. 229-266, 1996.
- [19] T. Lasheen, M. El-Ahmady, H. Hassib and A. Helal, "Molybdenum Metallurgy Review: Hydrometallurgical Routes to Recovery of Molybdenum from Ores and Mineral Raw Materials," *Mineral Processing & Extractive Metallurgy Review*, vol. 36, no. 3, pp. 145-173, 2015.
- [20] P. Garg, S.-J. Park and R. M. German, "Effect of die compaction pressure on densification behavior of molybdenum powders," *International Journal of Refractory Metals and Hard Materials*, vol. 25, no. 1, pp. 16-24, 2007.
- [21] S. Kumar and S. Pityana, "Laser-based additive manufacturing of metals," In *Advanced Materials Research*, vol. 227, pp. 92-95, 2011.
- [22] M. Attaran, "The rise of 3-D printing: The advantages of additive manufacturing over traditional manufacturing," *Business Horizons*, vol. 60, no. 5, pp. 677-688, 2017.

- [23] J. Kranz, D. Herzog and C. Emmelmann, "Design guidelines for laser additive manufacturing of lightweight structures in TiAl6V4," *Journal of Laser Applications*, vol. 27, p. S14001, 2015.
- [24] K. WE, B. HD, C. VM, G. GF, G. JW, H. DE and e. al., "Observation of keyhole-mode laser melting in laser powder-bed fusion additive manufacturing," *J Mater Process Technol*, vol. 214, no. 12, pp. 2915-2925, 2014.
- [25] T. DebRoy, H. L. Wei, J. S. Zuback, T. Mukherjee, J. W. Elmer, J. O. Milewski, A. M. Beese, A. E. Wilson-Heid, A. De and W. Zhang, "Additive manufacturing of metallic components – Process, structure and properties," *Progress in Materials Science*, vol. 92, pp. 112-224, 2018.
- [26] N. Aboulkhair, N. Everitt and C. Tuck, "Reducing porosity in AlSi10Mg parts processed by selective laser melting," *Addit Manufacturing*, vol. 1, pp. 77-86, 2014.
- [27] B. A, S. T and K. C, "Defect generation and propagation mechanism during additive manufacturing by selective beam melting," *Mater Process Technology*, no. 11, pp. 2522-2528, 2014.
- [28] K. Mumtaz and N. Hopkinson, "Top surface and side roughness of Inconel 625 parts processed using selective laser melting," *Rapid Prototyping*, pp. 96-103, 2009.
- [29] D. Bu and Y. Shen, "Balling phenomena in direct laser sintering of stainless steel powder: metallurgical mechanisms and control methods," *Materials & Design*, vol. 30, no. 8, pp. 2903-2910, 2009.

- [30] B. Vrancken, L. Thijs, J.-P. Kruth and J. V. Humbeeck, "Heat treatment of Ti6Al4V produced by Selective Laser Melting: Microstructure and mechanical properties," *Journal of Alloys and Compounds*, vol. 541, pp. 177-185, 2012.
- [31] N. T. Aboulkhair, I. Maskery, C. Tuck, I. Ashcroft and N. M. Everitt, "The microstructure and mechanical properties of selectively laser melted AlSi10Mg: The effect of a conventional T6-like heat treatment," *Materials Science and Engineering: A*, vol. 667, pp. 139-146, 2016.
- [32] D. Herzog, V. Seyda, E. Wycisk and C. Emmelmann, "Additive manufacturing of metals," *Acta Materialia*, vol. 117, pp. 371-392, 2016.
- [33] "Mlab cusing - Concept Laser," [Online]. Available: <https://www.concept-laser..>
- [34] "Buehler – Grinding and Polishing," [Online]. Available: <https://www.buehler.com/grinding-polishing.php>.
- [35] "Benchtop Muffler Furnace," [Online]. Available: <https://assets.omega.com/manuals/M2159.pdf>.
- [36] "Criterion® electromechanical test systems," [Online]. Available: <https://www.mts.com/en/products/materials/static-materials-test-systems/criterion-electromechanical>.
- [37] "Metlab Corporation," [Online]. Available: <https://metlabcorp.com/store/product/equipment/hot-mounting/metpress-a/>.
- [38] Joyce, "Field Emission Scanning Electron Microscope (Tescan MAIA3)," [Online]. Available: <https://www.polyu.edu.hk/umf/facility/mrc/110-field-emission-scanning-electron-microscope-tescan-maia3/>.

- [39] P. Moore and G. Booth, "Mechanical testing of welds," in *The Welding Engineer's Guide to Fracture and Fatigue*, Woodhead Publishing, 2015, pp. 113-141.
- [40] "Brinell / Knoop / Vickers Hardness Tester - Qness 60 A/A+ EVO," [Online]. Available: <https://www.qatm.com/products/hardness-testing/micro-hardness-tester/qness-60-a-evo/>.

REPORT DOCUMENTATION PAGE				<i>Form Approved OMB No. 074-0188</i>	
<p>The public reporting burden for this collection of information is estimated to average 1 hour per response, including the time for reviewing instructions, searching existing data sources, gathering and maintaining the data needed, and completing and reviewing the collection of information. Send comments regarding this burden estimate or any other aspect of the collection of information, including suggestions for reducing this burden to Department of Defense, Washington Headquarters Services, Directorate for Information Operations and Reports (0704-0188), 1215 Jefferson Davis Highway, Suite 1204, Arlington, VA 22202-4302. Respondents should be aware that notwithstanding any other provision of law, no person shall be subject to a penalty for failing to comply with a collection of information if it does not display a currently valid OMB control number.</p> <p>PLEASE DO NOT RETURN YOUR FORM TO THE ABOVE ADDRESS.</p>					
1. REPORT DATE (DD-MM-YYYY) 24-03-2022		2. REPORT TYPE Master's Thesis		3. DATES COVERED (From - To) March 2021 - March 2022	
TITLE AND SUBTITLE Investigation Of Additively Manufactured Molybdenum-Tungsten-Rhenium Alloys				5a. CONTRACT NUMBER	
				5b. GRANT NUMBER	
				5c. PROGRAM ELEMENT NUMBER	
6. AUTHOR(S) Abaya, Randolph T., Captain, USAF				5d. PROJECT NUMBER	
				5e. TASK NUMBER	
				5f. WORK UNIT NUMBER	
7. PERFORMING ORGANIZATION NAMES(S) AND ADDRESS(S) Air Force Institute of Technology Graduate School of Engineering and Management (AFIT/EN) 2950 Hobson Way, Building 640 WPAFB OH 45433-7765				8. PERFORMING ORGANIZATION REPORT NUMBER AFIT-ENY-MS-22-M-276	
9. SPONSORING/MONITORING AGENCY NAME(S) AND ADDRESS(ES) Air Force Research Laboratory				10. SPONSOR/MONITOR'S ACRONYM(S) AFRL/RXMS	
				11. SPONSOR/MONITOR'S REPORT NUMBER(S)	
12. DISTRIBUTION/AVAILABILITY STATEMENT DISTRUBTION STATEMENT A. APPROVED FOR PUBLIC RELEASE; DISTRIBUTION UNLIMITED.					
13. SUPPLEMENTARY NOTES This material is declared a work of the U.S. Government and is not subject to copyright protection in the United States.					
14. ABSTRACT The process of creating metal components through additive manufacturing is changing the way different industries can avoid the shortcomings of traditional metal production. Metals such as tungsten, molybdenum, and rhenium have many advantages for different applications, especially when alloyed together. In this study, an additively manufactured alloy containing 70% molybdenum, 25% tungsten, and 5% rhenium (70Mo-25W-5Re) is tested for its strength, ductility, hardness, and porosity. The 70Mo-25W-5Re alloy is printed through Laser Powder Bed Fusion (LPBF) under different conditions such as printing speed and printing atmosphere. Additionally, the effects of post printing heat treatment are conducted to understand the advantages to its property changes. The printed alloys are subject to flexural loading and its physical characteristics are tested and observed. The alloy is found to be stronger at slower printing speeds which corresponds to a greater input energy density. Additionally, heat treatments acted to improve strength but had little effect on porosity or hardness. The benefits of the 70Mo-25W-5Re alloy have a potential for real world applications due to its ease in production. The findings of this research demonstrated how readily alloys of these elements can be studied by leveraging additive manufacturing and post processing heat treatments. This technique will encourage research into different combinations of the constituent elements to find promising compositions in the alloy space.					
15. SUBJECT TERMS Additive Manufacturing, Selective Laser Melting, Laser Powder Bed Fusion, Molybdenum, Tungsten, Print Speed, Build Orientation, Post Processing Heat Treatment,					
16. SECURITY CLASSIFICATION OF:			17. LIMITATION OF ABSTRACT UU	18. NUMBER OF PAGES	19a. NAME OF RESPONSIBLE PERSON Ryan Kemnitz, AFIT/ENY
a. REPORT U	b. ABSTRACT U	c. THIS PAGE U			19b. TELEPHONE NUMBER (Include area code) (937) 255-3636, ext 4775; ryan.kemnitz@afit.edu

Standard Form 298 (Rev. 8-98)
Prescribed by ANSI Std. Z39-18

